Geochronology, 8, 255–277, 2026
https://doi.org/10.5194/gchron-8-255-2026

Paired ^{14}C–^{10}Be exposure ages from Mount Murphy, West Antarctica: Implications for accurate and precise deglacial chronologies

Jonathan R. Adams[1,2], Dylan H. Rood[1], Klaus Wilcken[3], Stephen J. Roberts[2], and Joanne S. Johnson[2]

[1]Department of Earth Science & Engineering, Imperial College London, Exhibition Road, London, SW7 2AZ, UK
[2]British Antarctic Survey, High Cross, Madingley Road, Cambridge, CB3 0ET, UK
[3]Australian Nuclear Science and Technology Organization, Lucas Heights, NSW 2234, Australia

Correspondence: Jonathan R. Adams (jonathan-richard.adams@univ-lorraine.fr)

Received: 28 November 2024 – Discussion started: 9 December 2024
Revised: 21 February 2026 – Accepted: 5 March 2026 – Published: 5 May 2026

Abstract. Cosmogenic-nuclide surface exposure ages provide empirical data for validating models simulating the timing and pace of ice-sheet response to a warming climate. Increasing emphasis is being placed on obtaining exposure ages that both accurately constrain Holocene deglaciation and are precise enough to capture ice sheet change at the sub-millennial scale. However, longer-lived nuclides such as ^{10}Be are susceptible to cosmogenic nuclide inheritance often persisting through multiple periods of exposure and burial, which can impact the accuracy of the most recent Holocene exposure history. Shorter-lived in situ cosmogenic ^{14}C (in situ ^{14}C) is largely insensitive to nuclide inheritance pre-dating the last glacial maximum (LGM), and when combined with longer-lived nuclides can be used to constrain complex ice sheet histories over Holocene timescales. Here, we present new in situ ^{14}C exposure ages from nine erratic cobbles from Mount Murphy, West Antarctica. Six of these suggest Mt Murphy deglaciated from 5–3 ka; this is inconsistent with previously measured ^{10}Be ages of the same samples that place deglaciation from 8–6 ka. We investigate potential explanations for the conflicting exposure histories by analysing paired ^{14}C–^{10}Be data of Holocene age presently archived in the informal cosmogenic-nuclide exposure-age database (ICE-D, https://version2.ice-d.org/, last access: 29 March 2024). Our analysis reveals that neither variations in geologic setting nor modelled scenarios of subsurface nuclide production can explain the conflicting Mt Murphy ages. However, replicate in situ ^{14}C measurements indicate that initial in situ ^{14}C concentrations used to calculate the youngest exposure ages (5–3 ka) do not reproduce within stated 2σ uncertainty, whereas measurements used to calculate the older ages (8–6 ka) are reproducible. Furthermore, we observe that in situ ^{14}C concentrations measured in 15 of 31 samples taken from ICE-D do not replicate within their nominal 2σ analytical uncertainty. Together, these results suggest that analytical uncertainty for in situ ^{14}C measurements may currently be underestimated. We provide recommendations for improving measurement precision that will benefit future Holocene deglaciation studies, including analysis and publication of more replicate measurements and the continuation of efforts to quantify and minimise sources of scatter in blank measurements.

1 Introduction

Increasing emphasis is being placed on glacial chronologies that both constrain the timing of ice-surface change during the Holocene epoch and provide validation for model simulations at sub-millennial scale resolution (Hippe, 2017; Johnson et al., 2022; Jones et al., 2022; Nichols et al., 2019). For model validation, cosmogenic radionuclide (e.g., in situ cosmogenic ^{14}C, hereafter in situ ^{14}C, and ^{10}Be) exposure ages must both be accurate and precise. Accurate determination of a Holocene exposure age relies on the assumption that the sample being dated is free from nuclides accumulated during periods of surface exposure that pre-date the LGM (Balco, 2011). The prevalence of cold-based ice and conse-

quent lack of basal erosion, however, often leads to nuclide inheritance where longer-lived nuclides such as ^{10}Be (half-life; 1.387 Myr) persist over multiple glacial cycles (Balco, 2011; Hein et al., 2014). The shorter half-life of in situ ^{14}C (5700±30 years) greatly reduces the impact of any pre-LGM exposure on ^{14}C exposure ages constraining the most recent deglaciation. For instance, a rock surface exposed prior to the LGM for long enough to reach in situ ^{14}C saturation (equilibrium between production and decay), deeply shielded by ice at 25 ka, and re-exposed at 10 ka would contain a pre-LGM in situ ^{14}C inventory that only accounted for ∼ 6 % of the in situ ^{14}C measured in that rock surface at the present day (Balco et al., 2019). In situ ^{14}C is therefore unique among cosmogenic nuclides for being largely insensitive to pre-LGM exposure, making it ideal for studying Holocene deglacial histories. However, measuring in situ ^{14}C in quartz is extremely challenging and was not routinely possible until relatively recently (Lifton et al., 2001).

Following efforts to develop and improve in situ ^{14}C extraction procedures (Fülöp et al., 2010, 2015, 2019; Goehring et al., 2014, 2019a; Hippe et al., 2009, 2013; Lamp et al., 2019; Lifton et al., 2001, 2015b, 2023; Lifton, 1997; Lupker et al., 2019), the method has been successfully applied to accurately determine Holocene exposure where ^{10}Be inheritance is known or suspected (Briner et al., 2014; Nichols et al., 2019; White et al., 2011). Combining analyses of short-lived in situ ^{14}C with longer-lived ^{10}Be has provided a valuable approach to detecting and quantifying complex exposure histories (Hippe, 2017). If measurement precision of both nuclides is sufficient to resolve past ice sheet behaviour at the sub-millennial timescale, then this method can be a powerful way of identifying and quantifying phases of retreat and readvance in the later Holocene, for which there is emerging evidence (Balco et al., 2023; Kingslake et al., 2018; Venturelli et al., 2020, 2023).

In this study, we present new in situ ^{14}C exposure ages measured in samples from Mt Murphy, a volcano adjacent to Thwaites Glacier in the Amundsen Sea Embayment (Fig. 1a). When compared to previously published ^{10}Be ages (Adams et al., 2022; Johnson et al., 2020), our new in situ ^{14}C ages apparently suggest two conflicting exposure histories at Mount Murphy. Some paired in situ ^{14}C–^{10}Be ages from the same sample are concordant (where the paired ^{14}C–^{10}Be ages agree within uncertainty), indicating the sample experienced a simple post-LGM exposure history. Others are discordant (the paired ^{14}C–^{10}Be ages do not overlap within analytical uncertainty), indicating that a sample experienced burial since post-LGM exposure or that there were changes in the nuclide production rate (Balco et al., 2019).

Here, we describe an investigation into potential explanations for co-existing concordant and discordant paired ^{14}C–^{10}Be Holocene exposure ages observed at Mt Murphy. We do this by revisiting the data of Johnson et al. (2020) and Adams et al. (2022), and performing a more in-depth examination of sources of uncertainty associated with both in situ ^{14}C and ^{10}Be exposure ages. First, we present a new in situ ^{14}C dataset from Mt Murphy (paired with previously published ^{10}Be measurements) (Fig. 1a) and assess the accuracy and reproducibility of this new dataset. We then perform a sensitivity analysis using blank and CRONUS-A quality control data (Table S5, Balco et al., 2023) and assess its impact on our new in situ ^{14}C data. Finally, we contextualise the new Mt Murphy dataset by analysing available ^{14}C–^{10}Be paired exposure age data that is of Holocene age (<∼ 11.7 ka) from Antarctica (Fig. 1b) and globally (Fig. 1c). These paired ^{14}C–^{10}Be data are primarily sourced from publicly available data archived in the Informal Cosmogenic-nuclide Exposure age Database (Balco, 2020b) (https://version2.ice-d.org/, last access: 29 March 2024). By documenting our rigorous investigation of a challenging paired in situ ^{14}C–^{10}Be dataset from Mt Murphy, West Antarctica, we aim to provide a conceptual framework with which the growing end-user community may better critically test, diagnose, and improve the accuracy and precision of future in situ ^{14}C cosmogenic exposure ages using multinuclide (e.g., in situ ^{14}C–^{10}Be) methods, and identify steps the community could take to consistently produce robust Holocene glacial chronologies.

1.1 Sources of uncertainty that impact in situ ^{14}C and ^{10}Be exposure ages

To provide additional context for our results and discussion, we first outline sources of uncertainty that need to be accounted for when calculating in situ ^{14}C and ^{10}Be exposure ages, and introduce the concept of paired nuclide diagrams (Granger, 2006). Uncertainty impacts both accuracy and precision at all stages of determining an exposure age of a sample and can be divided broadly into three categories: (i) geologic uncertainty (ii) uncertainty incorporated during sample preparation and isotopic analysis to determine a nuclide concentration and (iii) uncertainty sourced from exposure age calculations.

Cosmogenic nuclide practitioners have least control over geologic uncertainty, which is inherent in a sample from its time of collection in the field and rooted in the limited knowledge we have of a sample's true exposure history and any processes that may have modified production of nuclides following exposure (Dunai, 2010). The two main sources of geologic uncertainty are nuclide inheritance (described above) and post depositional disturbance caused by shielding, erosion, and/or rolling of a sample (Balco, 2011; Gosse and Phillips, 2001). Steps commonly taken to reduce their impact include a robust and detailed geologic interpretation of deposits or depositional features being dated (Balco, 2011) and statistical techniques (Heyman et al., 2016; Johnson et al., 2014). Comprehensive summaries of geologic uncertainty and efforts to quantify it can be found in Balco et al., (2011, 2020b).

The second major source of uncertainty comes from our ability to measure the nuclide concentration accurately and

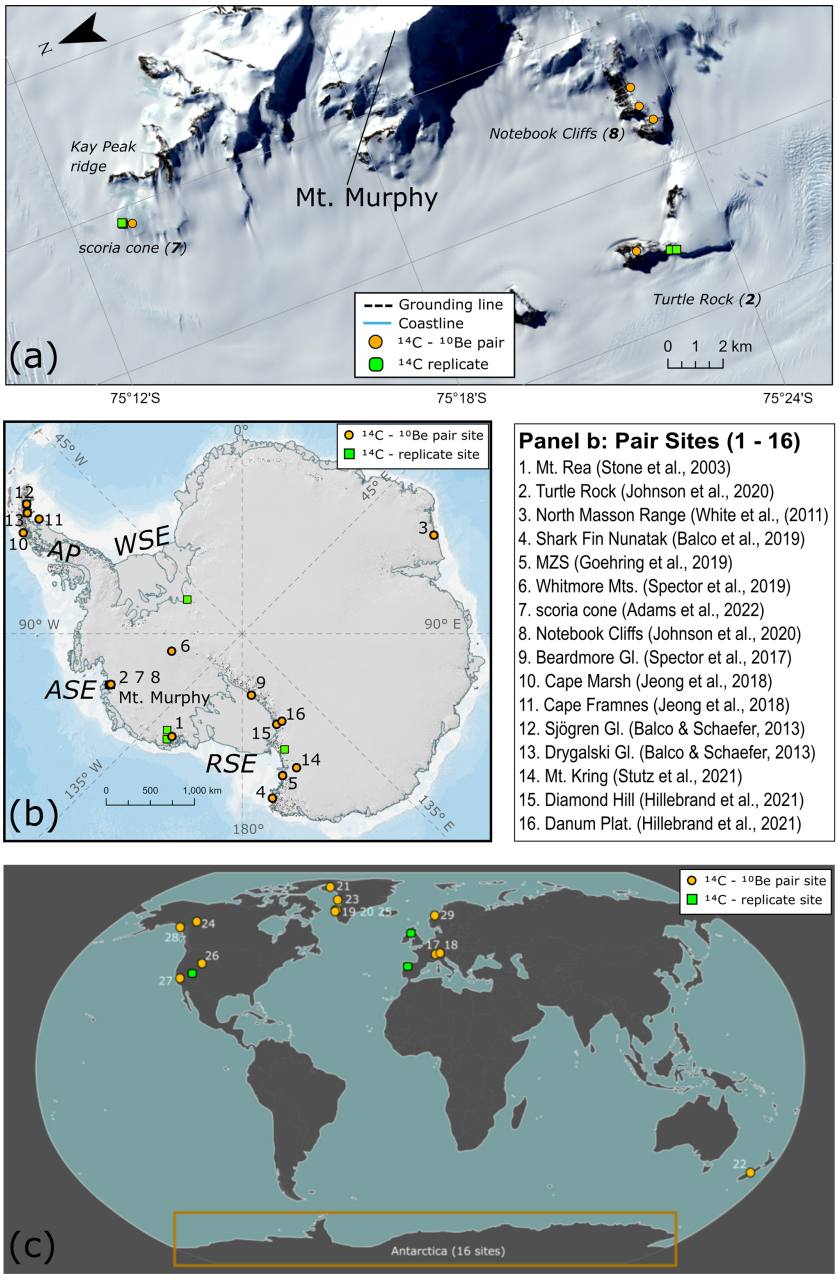

Figure 1. Panel **(a)** a Landsat-9 satellite image of the Turtle Rock, scoria cone and Notebook Cliffs sites at Mt Murphy showing locations of samples with new in situ ^{14}C exposure ages and previously published ^{10}Be exposure ages. Grounding line position uses data from (Milillo et al., 2022) and Antarctic Coastline is from version 7.7 of the Antarctic Digital Database. Panel **(b)** shows Antarctic and panel **(c)** global site locations of paired ^{14}C–^{10}Be ages (sites 1–29) where both: (i) apparent ^{10}Be exposure ages are $< 4\times$ older than apparent ^{14}C exposure ages (ii) ^{10}Be exposure ages are of Holocene age (< 11.7 ka) which are relevant to Sect. 4. of this manuscript but introduced here to better contextualise our results from Mt Murphy. Site numbering uses the order of the specific site ID (lowest to highest) that locations have been assigned in ICE-D (Balco, 2020b). Panel **(b)** Antarctic paired ^{14}C–^{10}Be site locations (1–16) are specified in an inset figure key. Panel **(b)** abbreviations indicate the Antarctic Peninsula (*AP*), Amundsen Sea Embayment (*ASE*), Ross Sea embayment (*RSE*) and Weddell Sea embayment (*WSE*). Details of global site locations (17–29) displayed in panel **(c)** are specified in Results, Table 4. Green squares in panel **(c)** indicate locations where multiple in situ ^{14}C measurements have been made on the same sample including Lake Bonneville, Utah, Northwest Highlands, Scotland and Leymon High, Northwest Spain (see Fig. 8 and Table S3 in the Supplement). Note in panel **(a)** the corresponding site number from the global site index (1–29) is specified in bold italics along with the name of the sample site, e.g., Turtle Rock (*2*). Note in panel **(b)** paired in situ ^{14}C–^{10}Be sites 2, 7, 11 and 13 also contain replicate in situ ^{14}C measurements but only the paired ^{14}C–^{10}Be symbol (orange circle) is displayed.

precisely within a sample, which represents the internal uncertainty component of an exposure age calculation (Balco, 2020a). Cosmogenic nuclide dating specialists make efforts to minimise contributions to measurement uncertainty particularly from i) uncertainties introduced during sample preparation, and ii) sample measurement by accelerator mass spectrometry (AMS). Measurement of the cosmogenic nuclide ^{10}Be is now relatively well-established and routine following efforts to reduce sources of laboratory sample preparation uncertainty (Corbett et al., 2016, 2022; Kohl and Nishiizumi, 1992) and improve AMS performance (Merchel et al., 2012; Rood et al., 2010, 2013; Wilcken et al., 2022). These efforts have resulted in ^{10}Be measurement precision on typical quartz interlaboratory comparison materials (e.g., CRONUS-A, CoQtz-N) of between $\sim 2\,\% - 4\,\%$ (Binnie et al., 2019; Jull et al., 2015; Phillips et al., 2016a). For high in situ ^{14}C concentrations ($\geq 1 - 2 \times 10^5$ at g^{-1}) internal analytical uncertainty is dominated by AMS counting statistics, with a total measurement uncertainty (combined AMS counting error and blank correction) averaging $< 2\,\%$ (Goehring et al., 2014; Hippe, 2017). For moderate in situ ^{14}C concentrations in the 10^4 at g^{-1} range, the uncertainty from AMS counting statistics increases, but typically remains below 10 % and mostly below 5 % (Hippe, 2017). However, for lower in situ ^{14}C concentrations the blank correction increasingly dominates, leading to a rapid increase in total uncertainty (Goehring et al., 2014; Hippe, 2017). These sources of uncertainty have been challenging to quantify despite improvements to in situ ^{14}C extraction from quartz (Fülöp et al., 2010, 2015, 2019; Goehring et al., 2014, 2019a; Hippe et al., 2009, 2013; Lamp et al., 2019; Lifton et al., 2001, 2015b, 2023; Lifton, 1997; Lupker et al., 2019) and the dominance of the blank at lower concentrations illustrates the significant challenges of avoiding contamination from other potential sources of C that impart uncertainty into the final in situ ^{14}C measurement. Laboratory intercomparison reproducibility studies of CRONUS-A (an intercomparison material for cosmogenic nuclides including ^{14}C and ^{10}Be) indicate the coefficient of variation (CoV) of in situ ^{14}C concentration measurements is in the range of 6 %–8 %, and 3 %–4 % for ^{10}Be (Phillips et al., 2016a). There have also been several recent improvements to the in situ ^{14}C extraction process, including identification of potential contaminant sources introduced during quartz purification (Nichols and Goehring, 2019), and automation of ^{14}C extraction lines that reduce risk of atmospheric ^{14}C contamination (Goehring et al., 2019a; Lifton et al., 2015b, 2023; Lupker et al., 2019). Refinements to the stepped heating process to liberate in situ ^{14}C (in the form of CO_2) from quartz are also being explored (Lifton et al., 2023) and some extraction facilities now omit the graphitisation stage (that converts CO_2 to C) in favour of analysing in situ ^{14}C directly using gas source AMS (e.g., Lamp et al., 2019).

The final major source of uncertainty comes from transforming a measured nuclide concentration into an exposure age. This requires estimating the production rate due to secondary spallation reactions, which accounts for the majority of surface production (Dunai, 2010), and muons (Balco, 2017). Production rate uncertainties have been incrementally reduced via improvements in scaling models, especially more recent models based on particle-physics simulations (Argento et al., 2015a, b; Lifton et al., 2014). Estimates of the ^{10}Be production rate uncertainty from spallation are currently in the range of 6 % (Borchers et al., 2016; Marrero et al., 2016). However, in the case of in situ ^{14}C, a spallogenic production rate uncertainty could not be fitted to calibration data because of scatter in excess of an assumed measurement uncertainty of 7.3 % for in situ ^{14}C concentrations at selected calibration sites (Borchers et al., 2016). Muons account for a much smaller proportion of total cosmogenic nuclide production at the surface than spallation, but this quantity differs between ^{10}Be and in situ ^{14}C. The proportion of ^{10}Be production by muons at the surface is between 1.5 %–2 %, which translates to a maximum scaling uncertainty of only 0.5 % for estimating total ^{10}Be surface production by muons. However, for in situ ^{14}C, production by muons accounts for $\sim 20\,\%$ of total in situ ^{14}C nuclide production at the surface (Lupker et al., 2015). Therefore, for in situ ^{14}C the same 10 %–25 % uncertainty on computing a production rate by muons equates to between a 2 % and maximum 5 % uncertainty on the total surface production rate estimate (Balco, 2017).

Due to the inherently different systematics of production and radioactive decay of in situ ^{14}C and ^{10}Be, paired nuclide diagrams (Fig. 2) represent a useful method of visualizing and interpreting exposure/burial histories, and can help to identify or explain uncertainty and scatter in a dataset (see Granger, 2006 for a detailed description of paired nuclide diagrams). Paired nuclide plots generated from exposure age pairs (including ^{14}C–^{10}Be pairs) can be classed into three distinct types: Type 1 for samples with simple exposure history (only one period of exposure), Type 2 for samples with a complex exposure history (multiple periods of exposure and burial), and Type 3 for samples with an impermissible concentration ratio (where an ellipse plots above the line of constant exposure in the "impermissible" zone). The Type 3 scenario can indicate analytical inconsistencies, for example, ^{14}C contamination increasing in situ ^{14}C concentrations (Nichols and Goehring, 2019) or could reflect application of an incorrect production rate to one or both nuclides. In certain cases, a Type 3 nuclide ratio may be explained geologically because the constant exposure line assumes a surface production rate rather than subsurface production. However, because the cosmogenic nuclide production rate by muons as a proportion of total surface production is an order of magnitude higher for in situ ^{14}C than for ^{10}Be, the ^{14}C–^{10}Be production ratio increases with depth below the surface (Hippe, 2017). For example, a sample that is buried under a thin layer of rock, ice, till or other material and then rapidly exhumed by plucking can, therefore, exhibit seemingly "impermissi-

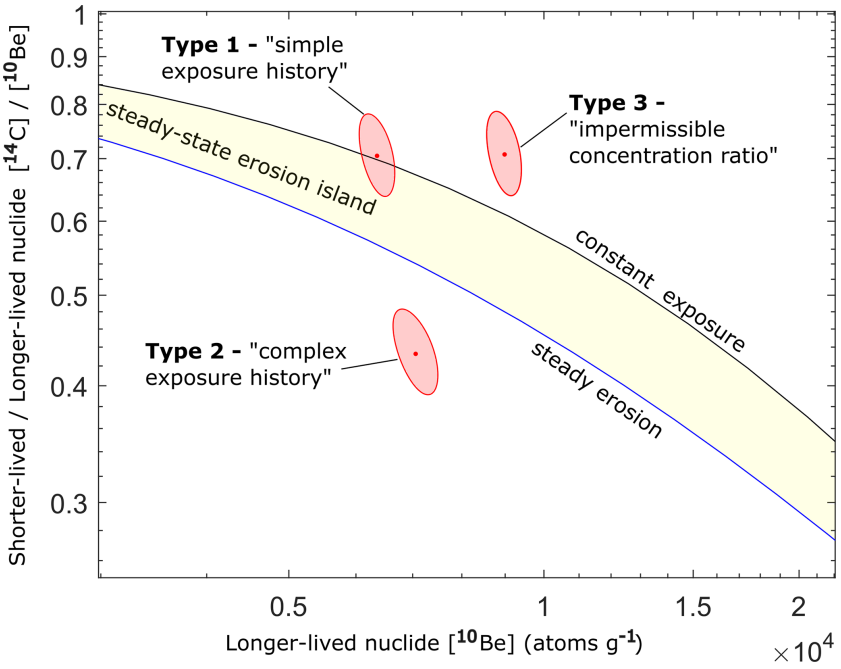

Figure 2. Paired nuclide diagram with key features labelled. Note that the x-axis includes the concentration of the longer-lived nuclide, in this case ^{10}Be, and the y-axis is the ratio of the concentration of the shorter- to longer-lived nuclide, in this case ^{14}C–^{10}Be. Both axes are normalised to the local nuclide production rate at each sample location using the LSDn scaling model. Uncertainty ellipses (68 % confidence) are plotted using code from the online calculators formerly known as the CRONUS-Earth online calculators (Balco et al., 2008). Constant exposure line (upper black), steady erosion line (lower blue), and steady-state erosion island (yellow shaded) are labelled on the figure. Paired nuclide diagram terminology from (Granger, 2006).

ble" paired ^{14}C–^{10}Be concentrations due to differences in the ^{14}C–^{10}Be total production ratio at the surface versus at depth (Hippe, 2017; Rand and Goehring, 2019).

In summary, sources of geologic, sample preparation, and exposure age calculation uncertainty impact the accuracy and precision of Holocene deglaciation chronologies. An increase in paired ^{14}C–^{10}Be measurements in the recent $\sim$ 5 years, driven by greater ^{14}C extraction throughput (Goehring et al., 2019a; Lifton et al., 2015b, 2023) provide many new data to make an assessment of the application of both nuclides and investigate sources of uncertainty, particularly of in situ ^{14}C. In the following sections, we investigate the cause of concordant and discordant paired in situ ^{14}C–^{10}Be exposure ages at Mt Murphy and potential causes for the large amounts of scatter in reported in situ ^{14}C measurements using new in situ ^{14}C data from Mt Murphy and existing paired in situ ^{14}C–^{10}Be data extracted from ICE-D.

2 Methods

2.1 Site description and sample selection

Mount Murphy is a large volcanic edifice adjacent to Thwaites Glacier in the Amundsen Sea Embayment (Fig. 1a). Along its western flank, adjacent to Pope Glacier, there are several smaller nunataks, many of which host erratic cobbles and boulders that are well-rounded and of exotic lithology, indicating transport to the site by ice. We selected nine samples from erratics (Table 1) for in situ ^{14}C analysis. These had previously been measured for ^{10}Be (Adams et al., 2022; Johnson et al., 2020), with the resultant thinning history implying exposure during the Holocene. We selected four of the nine samples for repeat in situ ^{14}C measurements to determine if measurement uncertainty may have contributed to conflicting exposure histories suggested by initial in situ ^{14}C concentrations from our samples.

We ensured that paired ^{10}Be and ^{14}C exposure ages cover a wide elevation range by selecting samples from three different locations around the Mt Murphy massif (Notebook Cliffs, samples collected from 893–834 m a.s.l. (metres above sea level), Turtle Rock, 696–438 m a.s.l., and a scoria cone adjacent to Kay Peak, 239–178 m a.s.l.). Notebook Cliffs comprises basaltic lava flows overlying thick sequences of hyaloclastite (Adams et al., 2025; Smellie, 2001). A few granite erratics and SSE–NNW trending bedrock striations are present, indicating past ice-cover (Johnson et al., 2020). Turtle Rock, situated adjacent to Pope Glacier, is primarily composed of hyaloclastite and consists of a broad flat lower terrace (438–452 m a.s.l.), which hosts the highest number of erratics observed at Mt Murphy (Johnson et al., 2020). Turtle Rock rises at its northern end to $\sim$ 710 m a.s.l. and consists of several superimposed sequences of basalt and hyalo-

Table 1. New in situ ^{14}C exposure ages from sites at Mt Murphy: Notebook Cliffs (NOT), Turtle Rock (TUR) and scoria cone (CIN). Exposure ages were calculated based on the blank correction reported from the Tulane CNL of $4.53 \pm 0.24 \times 10^4$ atoms for initial ^{14}C measurements ($n = 9$) and $7.14 \pm 0.30 \times 10^4$ atoms for replicate measurements using the LSDn scaling scheme. A nominal 6 % measurement uncertainty based on reproducibility of CRONUS-A reported from Tulane CNL of $6.12 \pm 0.32 \times 10^5$ at g^{-1} ($n = 10$) (Goehring et al., 2019a) is assigned to 1σ internal ^{14}C uncertainties and propagated into 1σ external uncertainties. Sample IDs appended with *R* denote repeat measurements. See Table S1 for full in situ ^{14}C AMS dataset. Previously published ^{10}Be ages measured from the same sample (Adams et al., 2022; Johnson et al., 2020) are included to facilitate comparison.

Sample ID	Latitude DD	Longitude DD	Elevation (m a.s.l.)	Lithology	^{10}Be Age (ka)	^{14}C Age (ka)	1σ Int. Err. (ka)	1σ Ext. Err. (ka)
NOT-104	−75.3886	−111.1175	893	granite	8.6	4.1	0.3	0.4
NOT-107	−75.3882	−111.0906	885	granite	8.9	5.2	0.4	0.6
NOT-103	−75.3914	−111.1399	852	granite	9.4	3.8	0.3	0.4
TUR-123	−75.3706	−111.2923	639	granite	10.3	3.8	0.3	0.4
TUR-117	−75.3811	−111.3066	451	granite	6.7	3.1	0.2	0.3
TUR-117-R	−75.3811	−111.3066	451	granite	–	8.2	0.8	1.1
TUR-132	−75.3830	−111.3091	446	granite	6.6	7.9	0.8	1.0
TUR-132-R	−75.3830	−111.3091	446	granite	–	7.4	0.7	0.9
CIN-102	−75.2194	−111.0232	239	gneiss	7.5	9.0	1.0	1.3
CIN-108	−75.2165	−111.0197	181	granite	6.2	6.3	0.6	0.7
CIN-108-R	−75.2165	−111.0197	181	granite	–	7.8	0.8	1.0
CIN-112	−75.2163	−111.0180	179	aplite	6.6	3.4	0.3	0.3
CIN-112-R	−75.2163	−111.0180	179	aplite	–	7.2	0.7	0.9

clastite, with erratics collected from three smaller terraces up to 696 m a.s.l. (Johnson et al., 2008, 2020). The scoria cone is located > 15 km downstream of Notebook Cliffs and Turtle Rock and is less than 1 km from the grounding line of Pope Glacier. The site consists of two small outcrops comprised of rubbly oxidised scoria bounded on one side by a moraine (Adams et al., 2022; Nichols et al., 2024). Cobbles deposited on the outcrops are generally well-rounded suggesting long distance transport (Adams et al., 2022). Detailed geological and geomorphological descriptions of these sites are provided by Johnson et al. (2020) and Smellie (2001). Geomorphic descriptions and supporting information of the nine samples with paired ^{14}C–^{10}Be measurements are provided in Sect. S1 and Table S2 in the Supplement.

2.2 In situ ^{14}C analysis of Mt Murphy samples

We obtained purified quartz necessary for in situ ^{14}C extraction of initial and replicate samples by performing mineral separation on our whole rock samples in the CosmIC Laboratory at Imperial College London (UK), largely following methods specified in Corbett et al. (2016). We omitted the froth flotation step (used to separate feldspars and quartz) following recommendations made by Nichols and Goehring (2019) and instead performed 3×1 % HF/HNO_3 etches to isolate the quartz (Kohl and Nishiizumi, 1992). Quartz purity was determined using Inductively Coupled Plasma Optical Emission Spectrometry (ICP-OES), after which ∼ 10 g of purified quartz from each sample was sent to Tulane University Cosmogenic Nuclides Laboratory (Tulane CNL, New Orleans, USA) for in situ ^{14}C extraction. Extraction of in situ ^{14}C was performed using the fully automated Tulane University Carbon Extraction and Graphitisation System (TU-CEGS) following methods presented in Balco et al. (2023), modified from Goehring et al. (2019a). Sample aliquots of purified quartz ranging from 3–5 g were loaded into platinum crucibles and fused with lithium metaborate ($LiBO_2$) flux to ensure sample dissolution and complete liberation of in situ ^{14}C (Lifton et al., 2001). The sample was heated in a stable high purity O_2 atmosphere for 30 min at 500 °C to remove atmospheric ^{14}C and organic contaminants. Following evacuation of the furnace and addition of new high purity O_2, the sample was further heated to 1100 °C for 3 h to completely dissolve the quartz and liberate in situ ^{14}C (in the form of CO_2). Liberated CO_2 was cryogenically purified before being collected in a measurement chamber, quantified monometrically and diluted with ^{14}C-free CO_2 to ensure a measurable sample size (Goehring et al., 2019a). CO_2 was graphitized using standard H_2 reduction methods over an Fe catalyst (Santos et al., 2004, 2007; Southon, 2007). Several changes were made to the configuration of the TU-CEGS prior to the replicate measurements ($n = 4$). Alterations included the introduction of a new compact borosilicate coil trap held at liquid nitrogen temperature (−196 °C) for trapping evolved CO_2 following quartz dissolution (Lifton et al., 2015b, 2023, 2001; Pigati et al., 2010), which replaced the previously installed variable temperature trap (Goehring et al., 2019a). A new mullite tube was also used for ^{14}C extraction due to failure of the previous tube; mullite tubes at Tulane CNL have previously been observed to undergo a "break in" period, during which initial ^{14}C blanks are higher

but often fall with continued use (Goehring et al., 2019a). $^{14}C/^{12}C$ isotope ratios were measured by AMS at the National Ocean Sciences Accelerator Mass Spectrometry Facility (NOSAMS) (Woods Hole, USA) using the methods described in Longworth et al. (2015). A small aliquot of 2–3 µg of C was removed for $\delta^{13}C$ analysis at the University of California Davis Stable Isotope Facility (see Table S1 in the Supplement). Data reduction to convert $^{14}C/^{12}C$ ratios to $^{14}C/C_{total}$ followed methods outlined in Hippe and Lifton, (2014). We applied the blank correction reported from the Tulane CNL of $4.53 \pm 0.24 \times 10^4$ atoms for initial ^{14}C measurements ($n = 9$) and $7.14 \pm 0.30 \times 10^4$ atoms for replicate measurements ($n = 4$, Table S1), respectively, to total measured in situ ^{14}C concentrations. Prior to calculating exposure ages, we assigned a 6 % (1σ) uncertainty to each in situ ^{14}C measurement concentration reported by AMS. This 6 % uncertainty exceeds the reported analytical uncertainty for all in situ ^{14}C measurements made for this study and reflects the reproducibility of replicate measurements of CRONUS-A extracted at Tulane CNL, which is reported as $6.12 \pm 0.32 \times 10^5$ at g^{-1} ($n = 10$) (Goehring et al., 2019a). This 6 % uncertainty has been routinely applied by studies where in situ ^{14}C extraction was carried out at Tulane CNL, e.g., (Nichols et al., 2019).

We calculated exposure ages for the new in situ ^{14}C measurements, as well as for the published ^{10}Be measurements, using version 3 of the online calculators (https://hess.ess.washington.edu/math/v3/v3_age_in.html, last access: 10 September 2025) with the "LSDn" production rate scaling method for neutrons, protons, and muons (following Lifton et al., 2014 and summarised in Balco, 2017). For ^{10}Be, exposure ages were calculated based on the CRONUS-Earth primary production rate calibration data set of Borchers et al. (2016). For in situ ^{14}C, we used the long-term CRONUS-A measurements from extractions performed at Tulane CNL presented in Goehring et al. (2019a) for production rate calibration. When comparing in situ ^{14}C and ^{10}Be exposure ages at Mt Murphy, we used the external uncertainty, which includes the 6 % (1σ) measurement uncertainty propagated in quadrature with the production rate and scaling scheme uncertainties. We report all exposure ages assuming no erosion or snow cover (making them "apparent" exposure ages) and a sample density of 2.7 g cm^{-3} to maintain consistency with Johnson et al. (2020) and Adams et al. (2022). In situ ^{14}C AMS data and corresponding calculated exposure ages are available from the NERC UK Polar Data Centre, https://doi.org/10.5285/dbb30962-bbf3-434a-9f27-6de2f61a86e2 (Adams et al., 2024).

3 Results

3.1 In situ ^{14}C exposure ages from Mt Murphy

Thirteen in situ ^{14}C measurements (including four replicate measurements) were performed on nine erratic samples recovered from Notebook Cliffs, Turtle Rock, and the unnamed scoria cone (all from surfaces situated between 179 and 893 m a.s.l.). Exposure ages calculated from nuclide concentrations (Table 1) are reported with 1σ internal uncertainties unless otherwise stated. Initial in situ ^{14}C exposure ages from the nine samples range from 9.0 ± 1.0 ka to 3.1 ± 0.2 ka (Table 1 and Fig. S9 in the Supplement), with an average exposure age of 6.0 ± 2.1 ka (mean and standard deviation). At the unnamed scoria cone, in situ ^{14}C exposure ages exhibit considerable scatter over a small elevation range (180–240 m a.s.l.) with ages ranging from 9.0 ± 1.0 ka to 3.4 ± 0.3 ka. The spread of in situ ^{14}C exposure ages calculated from initial measured in situ ^{14}C concentrations is ~ 6 kyr, and some samples at higher elevations yield younger exposure ages than samples from lower elevations, which is the inverse of the expected age-elevation pattern associated with ice-sheet thinning through time. Apparent exposure ages from Notebook Cliffs (850–900 m a.s.l.) are 2 kyr younger than those from the scoria cone (180–240 m a.s.l.).

Repeat in situ ^{14}C measurements ($n = 4$) were made on samples TUR-117 and TUR-132 from Turtle Rock (450–650 m a.s.l.), and samples CIN-108, and CIN-112 from scoria cone (180–240 m a.s.l.) to determine if measurement reproducibility contributed to the two conflicting exposure histories suggested by initial in situ ^{14}C concentrations. Exposure ages calculated from the four repeat measurements range from 8.2 ± 0.8 ka to 7.2 ± 0.7 ka (Table 1). Only one exposure age derived from replicate measurements reproduce within internal measurement uncertainties (at 1σ), whilst three do not. Ages from TUR-117 and CIN-112 do not reproduce within internal uncertainty at 1σ (Table 1) or indeed 2σ, with ages calculated from initial ^{14}C concentrations resulting in ages 5–3 kyr younger than those calculated from replicate in situ ^{14}C measurements. In other words, TUR-117-R and CIN-112-R are 165 % and 112 % older, respectively, than initial ages from the same samples, and exhibit significant scatter in excess of their internal uncertainties. CIN-108-R (7.8 ± 0.8 ka) is 24 % older than CIN-108 (6.3 ± 0.6 ka) and does not reproduce within 1σ internal uncertainty. TUR-132-R does, however, reproduce within 1σ internal uncertainty. Neither Turtle Rock nor scoria cone sites show a systematic bias in terms of reproducibility, with each site yielding one unreproducible in situ ^{14}C exposure age. There is no correlation between sample lithology and in situ ^{14}C reproducibility, as ages derived from both granite and gneiss samples do not reproduce within internal uncertainties. Notably, initial analyses of samples from Notebook Cliff ($n = 3$) and TUR-123 from > 600 m a.s.l. all yield younger ages than those obtained from repeat measurements on samples below 500 m a.s.l.; this is inconsistent with the expected age-elevation pattern associated with ice thinning.

Published ^{10}Be exposure ages and initial in situ ^{14}C exposure ages from samples TUR-132, CIN-102 and CIN-108 overlap within their respective 1σ external uncertainties making them concordant (Fig. 3a). However, most of the

paired ^{14}C–^{10}Be ages ($n = 6$, including all Notebook Cliff samples, TUR-117, TUR-123, and CIN-112) are discordant and have apparent exposure ages that are mid-late Holocene (5–3 ka). Where in situ ^{14}C and ^{10}Be ages are concordant, the in situ ^{14}C age is systematically older and early- to mid-Holocene (9–6 ka). Ages calculated from three of four replicate measurements overlap at 1σ external uncertainty with the corresponding ^{10}Be exposure ages (Fig. 3b). However, the exposure age calculated from the in situ ^{14}C concentration of sample CIN-108-R is discordant with the ^{10}Be exposure age from the same sample. We note the initial in situ ^{14}C measurement of CIN-108 (6.3 ± 0.7 ka), and average of the two in situ ^{14}C measurements of CIN-108 (7.1 ± 0.9 ka, $n = 2$) resulted in a concordant ^{14}C–^{10}Be exposure age pair.

Based on their initial in situ ^{14}C concentrations, the samples from Notebook Cliffs, Turtle Rock, and scoria cone (Fig. 4a) can be classified as Type 1 and Type 2 nuclide ratios on a paired nuclide diagram (see Sect. 1.1). TUR-132, CIN-102 and CIN-108 plot within the steady-state erosion island (Type 1) and display concordant in situ ^{14}C and ^{10}Be exposure ages (Fig. 4a). The remaining samples (NOT-103, NOT-104, TUR-123, TUR-117, and CIN-112) yield paired ^{14}C and ^{10}Be nuclide concentrations that plot below the steady state erosion line, suggesting complex exposure histories (Type 2). Samples plotting below the steady erosion line ($n = 6$) include all the young in situ ^{14}C ages, which are discordant with respect to the ^{10}Be exposure age from the same sample. Conversely, all in situ ^{14}C concentrations measured in replicates result in older ^{14}C exposure ages and yield ^{14}C–^{10}Be ratios which plot within the steady state erosion island (Fig. 4b), suggesting samples CIN-112 and TUR-117 instead experienced a simple (Type 1) rather than complex (Type 2) exposure history. The ^{14}C–^{10}Be ratio of CIN-108-R, and to some extent TUR-117-R, CIN-102 and TUR-132, suggest Type 1 exposure but border on an impermissible Type 3 exposure history (see Fig. 2).

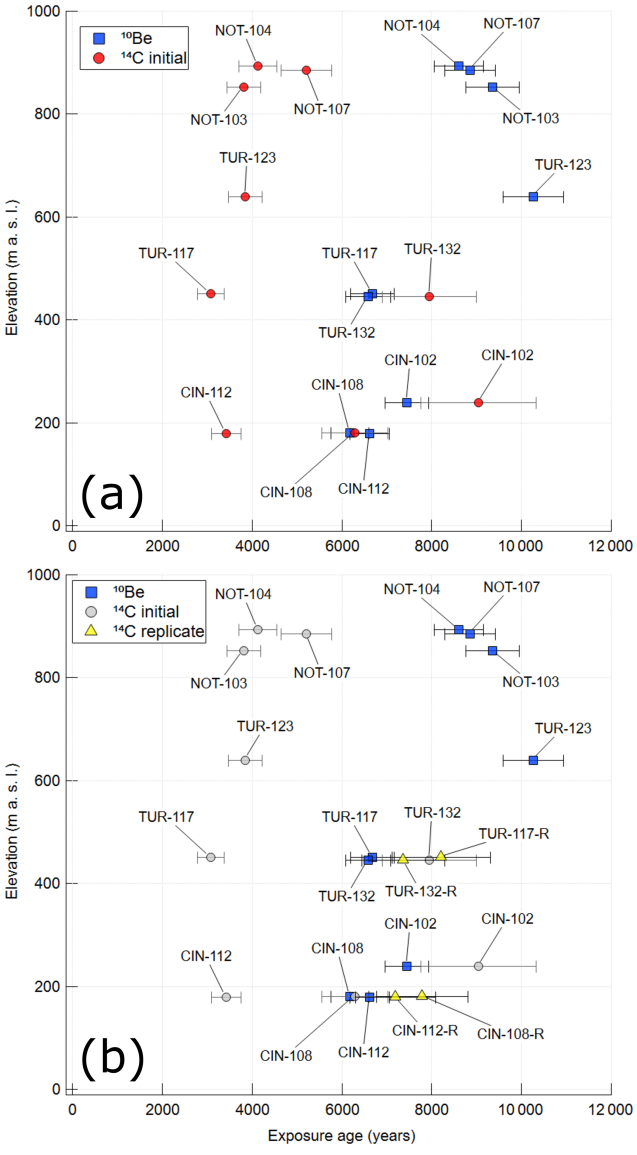

Figure 3. Mt Murphy paired ^{14}C–^{10}Be exposure age versus elevation plots **(a)** calculated using initial in situ ^{14}C concentrations and **(b)** using both initial (greyed-out) and replicate in situ ^{14}C concentrations. In situ ^{14}C exposure ages plotted with 1σ external uncertainties following application of nominal 6 % in situ ^{14}C measurement uncertainties. We report exposure ages with 1σ external uncertainties when comparing exposure ages calculated from in situ ^{14}C and ^{10}Be concentrations measured in the same sample (see Methods Sect. 2.2).

4 Discussion

4.1 Key observations from the Mt Murphy paired ^{14}C–^{10}Be exposure ages

Three of the four replicate in situ ^{14}C measurements yielded exposure ages that do not overlap within internal uncertainty (1σ). TUR-117-R and CIN-112-R also do not overlap at 2σ internal uncertainty with the corresponding initial ^{14}C exposure ages, and are also discordant with ^{10}Be exposure ages from the same samples. The six systematically young initial in situ ^{14}C exposure ages measured in samples ranging from 150–900 m a.s.l. appear to contradict previous interpretations of ice surface lowering to $\sim$ 150 m a.s.l. at Mt Murphy by 6 ka (Adams et al., 2022; Johnson et al., 2020). In addition, the young discordant in situ ^{14}C exposure ages from higher elevations (Notebook Cliffs and Turtle Rock upper terrace; TUR-123) and older reproducible in situ ^{14}C ages from lower elevations (scoria cone; CIN-102, CIN-108) contradict the age-elevation pattern expected with ice thinning. The two samples measured for in situ ^{14}C that did reproduce within their uncertainties at 2σ (TUR-132 and CIN-108) were also concordant with respect to ^{10}Be exposure ages from the same sample (Fig. 3b). From the Mt Murphy replicate measurements ($n = 4$), the two young in situ ^{14}C ages are not reproducible at 2σ internal uncertainty, but

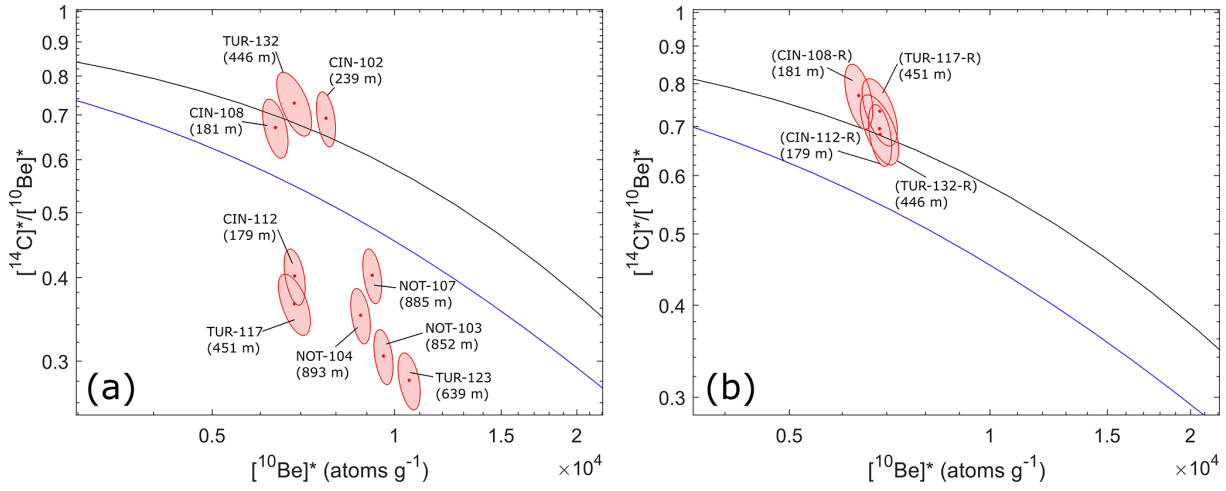

Figure 4. Paired ^{14}C–^{10}Be nuclide diagrams using new in situ ^{14}C concentrations from Mt Murphy samples. Panel **(a)** shows ^{14}C–^{10}Be nuclide ratios using initial in situ ^{14}C concentrations and panel **(b)** shows ^{14}C–^{10}Be ratios using in situ ^{14}C concentrations from repeat measurements. The x-axis represents the ^{10}Be concentration normalised to its production rate (at g^{-1} yr^{-1}) and the y-axis represents the ratio of the concentration of ^{14}C, the shorter half-life nuclide, normalised by its production rate to ^{10}Be – the longer-lived nuclide. All paired ^{14}C–^{10}Be concentration ratios are normalised to the sample-specific production rate using the LSDn scaling scheme and plotted as ellipses at 68 % confidence (Lifton et al., 2014) using the CRONUS-Earth calibration dataset for ^{10}Be (Borchers et al., 2016) and measurements of CRONUS-A at Tulane CNL for in situ ^{14}C (Goehring et al., 2019a). The asterisk indicates that the respective nuclide concentrations have been normalized to their respective production rates.

both older exposure ages are reproducible at 2σ internal uncertainty. In summary, Mt Murphy paired ^{14}C–^{10}Be exposure ages display both concordance and discordance across multiple sites. Concordant exposure ages are consistent with Type 1 ^{14}C–^{10}Be ratios and discordant exposure ages consistent with Type 2 ^{14}C–^{10}Be ratios. Concordant ^{14}C–^{10}Be exposure ages exhibit in situ ^{14}C ages which are reproducible at 2σ internal uncertainty whereas discordant ^{14}C–^{10}Be exposure ages do not. This lack of reproducibility suggests the stated 6 % (1σ) measurement uncertainty (based on replicability measurements of CRONUS-A at the in situ ^{14}C extraction laboratory) that is assigned to in situ ^{14}C concentrations prior to calculating an exposure age may be underestimated for our study.

A bootstrap linear regression analysis (see Sect. S3 in the Supplement) of in situ ^{14}C and ^{10}Be exposure age datasets from the scoria cone adjacent to Kay Peak indicate that the chronologies derived from each dataset are broadly similar with respect to the timing of deglaciation, implying they are equally accurate (see Fig. S14 in the Supplement). There is, however, excess scatter of $\sim$ 1849 years in the in situ ^{14}C ages (Sect. S3, Table S6 in the Supplement) that cannot be accounted for by the nominal 6 % 1σ internal measurement uncertainty for in situ ^{14}C that has been adopted in many studies (Balco et al., 2019; Nichols et al., 2019). Together, our new in situ ^{14}C exposure ages, the existing ^{10}Be exposure data and the corresponding ^{14}C–^{10}Be ratios from Mt Murphy (Figs. 3 and 4) raise two questions: (1) Is there a way to explain why 3 of the 4 replicate in situ ^{14}C analyses from Mt Murphy do not reproduce at 1σ internal uncertainties? and (2) Is there a geological explanation for the coexistence, often at the same elevation, of concordant and discordant paired in situ ^{14}C and ^{10}Be exposure ages? We discuss answers to these questions in the following sections.

4.2 Reanalysis of Mt Murphy in situ ^{14}C exposure ages using quality control data

First, we explore if discordant paired in situ ^{14}C–^{10}Be ages and in situ ^{14}C concentrations that do not reproduce within reported uncertainties can be explained by a comprehensive examination of blank and CRONUS-A data. For this, we describe results of a series of sensitivity analyses using quality control data from Tulane CNL (Balco et al., 2023).

For initial in situ ^{14}C concentrations, we apply a new blank correction of $7.44 \pm 4.16 \times 10^4$ atoms ($n = 6$, cf. Table S5 Balco et al., 2023) calculated from the mean and standard deviation of process blanks reported from 2 March–10 April 2021, which brackets the extraction dates of initial in situ ^{14}C measurements. For replicate in situ ^{14}C concentrations (extracted week beginning 19 April 2022), we apply a revised blank correction of $7.14 \pm 3.50 \times 10^4$ atoms, which is the same as reported from Tulane CNL. We also propagate a larger blank uncertainty of 35 043 atoms based on the standard deviation of all process blanks measured at Tulane CNL from 2019–2021 (Table S5, Balco et al., 2023). The blank uncertainty we use for the in situ ^{14}C replicate analyses is an order of magnitude larger than the blank uncertainty of $\sim$ 3000 atoms originally reported by Tulane CNL. See Sect. S2

in the Supplement, for a further sensitivity analysis using an alternative blank correction of $3.99 \pm 1.25 \times 10^4$ atoms ($n = 5$).

Prior to calculating in situ ^{14}C exposure ages, we also assign a 10 % (1σ) uncertainty to in situ ^{14}C concentrations calculated from the standard deviation of in situ ^{14}C measured in CRONUS-A extracted at Tulane CNL from 22 December 2015–12 March 2021 ($5.88 \pm 0.59 \times 10^5$ at g^{-1}, $n = 18$, cf. Table S5 Balco et al., 2023). For three in situ ^{14}C measurements, the 10 % value is exceeded by our combined AMS and recalculated blank uncertainty, which we use instead for the ^{14}C exposure age calculations (see Table 2 and Table S4 in the Supplement). The 10 % uncertainty we assign to in situ ^{14}C concentrations from the Mt. Murphy samples includes more recent measurements of CRONUS-A from Tulane CNL and is larger than the 6 % typically assigned to in situ ^{14}C measurements from that laboratory in other studies (e.g., Balco et al., 2019, Nichols at al., 2019, Rand et al., 2025).

Using different blank corrections (Table 2) to calculate the in situ ^{14}C exposure ages results in some improvements in reproducibility. Older initial in situ ^{14}C ages and replicate in situ ^{14}C ages in the $\sim 8-6$ ka range now all reproduce at 1σ and are concordant with previously published ^{10}Be ages. However, young initial in situ ^{14}C ages spanning from $\sim 5-3$ ka ($n = 6$) do not reproduce at 1σ (or 2σ) and remain discordant with published ^{10}Be ages (Fig. 5). The mean value of all initial in situ ^{14}C exposure ages lowers from 5.2±2.1 ka to 4.8 ± 2.0 ka when the larger blank correction is applied ($7.44 \pm 4.16 \times 10^4$ atoms). This shift to younger in situ ^{14}C ages increases the mismatch between TUR-117 and TUR-117R by 6.8 %, and CIN-108 and CIN-108-R by 10 %.

4.2.1 CRONUS-A normalization – sensitivity test

We conduct a further sensitivity test by normalizing our recalculated in situ ^{14}C concentrations (Table 3) using two different CRONUS-A datasets from Tulane (Table S5, Balco et al., 2023). First, we normalize the recalculated in situ ^{14}C concentrations (Table 2) using a CRONUS-A value of $5.88 \pm 0.59 \times 10^5$ at g^{-1} ($n = 18$) – calculated from the mean of all CRONUS-A from Tulane CNL – which is 4 % lower than the $6.12 \pm 0.32 \times 10^5$ at g^{-1} value reported in Goehring et al. (2019a). Second, we normalize Mt Murphy in situ ^{14}C concentrations to a CRONUS-A value of $7.11 \pm 0.10 \times 10^5$ at g^{-1}, which is 16 % higher. We select the higher value of $7.11 \pm 0.10 \times 10^5$ at g^{-1} firstly because it is the CRONUS-A value reported from Tulane CNL closest in time (12 March 2021) to the extraction of initial in situ ^{14}C measurements (2 March–10 April 2021), and secondly because it is the last CRONUS-A data published from Tulane CNL. In addition, it aligns more closely to the CRONUS-A value reported from other in situ ^{14}C extraction laboratories (see Table 5). The results of our sensitivity analyses are presented in Table 3, and Fig. S11 in the Supplement.

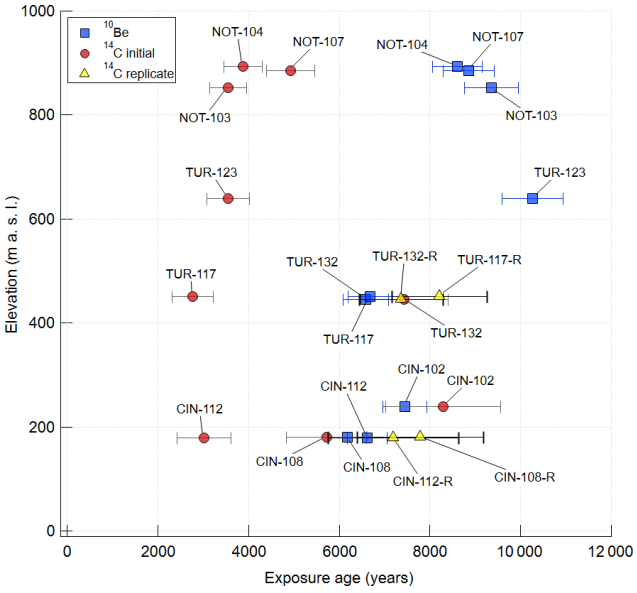

Figure 5. Mt Murphy paired ^{14}C–^{10}Be exposure age versus elevation plot showing ^{10}Be exposure ages and new in situ ^{14}C exposure ages calculated from initial and replicate in situ ^{14}C concentrations. Initial in situ ^{14}C concentrations use a blank correction of $7.44 \pm 4.16 \times 10^4$ atoms which brackets ^{14}C extraction dates from 2 March 2021–10 April 2021. Replicate in situ ^{14}C concentrations (yellow triangles) are calculated from the blank correction supplied by Tulane CNL for the samples of $7.14 \pm 3.50 \times 10^4$ atoms. We report exposure ages with 1σ external uncertainties when comparing exposure ages calculated from in situ ^{14}C and ^{10}Be concentrations measured in the same sample (see Methods Sect. 2.2). Our 1σ external uncertainty includes propagation of a 10 % uncertainty for in situ ^{14}C concentrations based on the standard deviation of CRONUS-A measurements reported at Tulane CNL from 2015–2021 ($n = 18$, cf. Table S5, Balco et al., 2023). The propagated AMS and blank uncertainties exceed 10 % for three in situ ^{14}C concentrations (see Table 2) and were used to calculate exposure age uncertainties for those samples.

Normalizing our in situ ^{14}C concentrations by a CRONUS-A value of $5.88 \pm 0.59 \times 10^5$ at g^{-1} (Fig. S11a) results in the young discordant in situ ^{14}C ages becoming an average of 12 % younger ($n = 6$) than those calculated using the original blank and normalized to the CRONUS-A value of $6.12 \pm 0.32 \times 10^5$ at g^{-1} (Table 1 and Sect. 3.1). Young ^{14}C ages are between 6.3 % (TUR-123) and 14.3 % (CIN-112) more discordant when compared with the corresponding ^{10}Be ages; however, the concordance and in situ ^{14}C reproducibility of the three older in situ ^{14}C ages improves, with CIN-108 and CIN-108-R overlapping within 1σ internal uncertainty. Normalizing in situ ^{14}C concentrations by a CRONUS-A value of $7.11 \pm 0.10 \times 10^5$ at g^{-1} has the opposite effect, with young discordant in situ ^{14}C ages becoming between 6.6 % (TUR-117) and 24.3 % (NOT-107) closer to the published ^{10}Be ages. Nevertheless, all the young in situ ^{14}C ages remain discordant with the ^{10}Be ages at 1σ and

Table 2. In situ ^{14}C concentration data measured in Mt Murphy samples. In situ ^{14}C concentrations are calculated from the mean and standard deviation of process blank data from Table S5 Balco et al. (2023), see Table S4 in the Supplement. The final column displays a 10 % assigned uncertainty for in situ ^{14}C concentrations based on the standard deviation of CRONUS-A measurements reported at Tulane CNL from 2019–2021 ($n = 18$, cf. Table S5 Balco et al., 2023). The 10 % uncertainty is assigned to situ ^{14}C concentrations prior to exposure age calculations when it exceeds the combined uncertainty calculated from ^{14}C AMS measurements and process blanks.

Sample ID (aliquot)	Blank Correction (atoms)	Blank Uncertainty (atoms)	Total ^{14}C (atoms)	$\pm 1\sigma$ (atoms)	^{14}C concentration (at g^{-1})	$\pm 1\sigma$ (at g^{-1})	± 10 % uncertainty (at g^{-1})
NOT-104-a	7.44×10^4	4.16×10^4	6.12×10^5	42 859	120 792	8465	12 079
NOT-107-a	7.44×10^4	4.16×10^4	7.07×10^5	43 375	144 739	8876	14 474
NOT-103-a	7.44×10^4	4.16×10^4	5.44×10^5	42 679	110 005	8624	11 001
TUR-123-a	7.44×10^4	4.16×10^4	4.63×10^5	42 613	92 300	8497	9230
TUR-117-a	7.44×10^4	4.16×10^4	3.27×10^5	42 148	64 290	8287	6429
TUR-117-b	7.14×10^4	3.50×10^4	6.77×10^5	36 900	140 624	7669	14 062
TUR-132-a	7.44×10^4	4.16×10^4	6.80×10^5	43 301	133 163	8477	13 316
TUR-132-b	7.14×10^4	3.50×10^4	6.29×10^5	36 897	132 368	7767	13 237
CIN-102-a	7.44×10^4	4.16×10^4	5.89×10^5	43 063	117 501	8594	11 750
CIN-108-a	7.44×10^4	4.16×10^4	4.45×10^5	42 465	87 545	8360	8754
CIN-108-b	7.14×10^4	3.50×10^4	3.77×10^5	35 901	107 288	10 217	10 729
CIN-112-a	7.44×10^4	4.16×10^4	2.73×10^5	42 067	54 330	8385	5433
CIN-112-b	7.14×10^4	3.50×10^4	3.10×10^5	35 708	102 114	11 777	10 211

Table 3. Comparison of recalculated in situ ^{14}C exposure ages from sites at Mt Murphy: Notebook Cliffs (NOT), Turtle Rock (TUR) and scoria cone (CIN). ^{14}C age (4th column) are the same values as in Table 1. The initial in situ ^{14}C concentrations used to calculate "Recalc. ^{14}C Age" use a new blank correction of $7.44 \pm 4.16 \times 10^4$ atoms and replicate in situ ^{14}C concentrations are again calculated from the blank correction supplied by Tulane CNL (7.14×10^4 atoms), but with an uncertainty calculated from the standard deviation of process blanks measured at Tulane CNL from 2019–2021 ($7.14 \pm 3.50 \times 10^4$ atoms). Additional sensitivity analyses that normalize our recalculated in situ ^{14}C concentrations by different CRONUS-A values are presented in column "S1 ^{14}C Age" (CRONUS-A; $5.88 \pm 0.59 \times 10^5$ at g^{-1} ($n = 18$)) and column "S2 ^{14}C Age" (CRONUS-A; $7.11 \pm 0.10 \times 10^5$ at g^{-1}), respectively. Sample IDs appended with R denote repeat measurements. See Table S1 for full in situ ^{14}C AMS results and Table S4 for calculations using Tulane CNL quality control data. The 1σ internal and external uncertainties for the S1 ^{14}C age and S2 ^{14}C age columns can also be found in Table S4, Sheet 4.

Sample ID	Elevation (m a.s.l.)	^{10}Be age (ka)	^{14}C Age (ka)	Recalc. ^{14}C Age (ka)	1σ Inter. Err. (ka)	1σ Exter. Err. (ka)	S1 ^{14}C Age (ka)	S2 ^{14}C Age (ka)
NOT-104	893	8.6	4.1	3.9	0.5	0.6	3.7	4.8
NOT-107	885	8.9	5.2	4.9	0.7	0.8	4.7	6.1
NOT-103	852	9.4	3.8	3.6	0.4	0.5	3.4	4.4
TUR-123	639	10.3	3.8	3.5	0.4	0.5	3.4	4.3
TUR-117	451	6.7	3.1	2.8	0.4	0.5	2.6	3.3
TUR-117-R	451	–	8.2	8.2	1.4	1.6	7.7	11.0
TUR-132	446	6.6	7.9	7.4	1.2	1.3	7.0	9.6
TUR-132-R	446	–	7.4	7.4	1.2	1.3	6.9	9.5
CIN-102	239	7.5	9.0	8.3	1.4	1.6	7.7	11.1
CIN-108	181	6.2	6.3	5.7	0.8	0.9	5.4	7.2
CIN-108-R	181	–	7.8	7.8	1.3	1.4	7.3	10.2
CIN-112	179	6.6	3.4	3.0	0.6	0.6	2.9	3.6
CIN-112-R	179	–	7.2	7.2	1.3	1.4	6.8	9.3

2σ uncertainty. Furthermore, the older in situ ^{14}C ages and replicates are now also discordant with ^{10}Be exposure ages (Fig. S11b).

Normalizing initial in situ ^{14}C concentrations by the CRONUS-A value of $7.11 \pm 0.10 \times 10^5$ at g^{-1} and replicate in situ ^{14}C concentrations by the CRONUS-A value of $5.88 \pm 0.59 \times 10^5$ at g^{-1} does not improve reproducibility of the young discordant in situ ^{14}C ages. In addition, the older initial in situ ^{14}C ages ($n = 3$) also do not reproduce at 1σ when this value is used (Fig. S11c). In summary, using the quality control data from Tulane and different blank corrections, assigning a larger uncertainty of 10 % to our in situ ^{14}C

concentrations and normalizing them to a CRONUS-A value of $5.88 \pm 0.59 \times 10^5$ at g^{-1} do slightly improve reproducibility of the older in situ ^{14}C ages. They also increase concordance with the ^{10}Be ages. However, neither a reasonable range of blank corrections nor normalization to a range of plausible CRONUS-A values can explain the lack of reproducibility associated with the six anomalously young initial in situ ^{14}C ages.

4.3 Potential sources of geological uncertainty

Instances of concordant and discordant ^{10}Be and ^{14}C exposure ages (Balco et al., 2019) or seemingly impermissible ^{14}C–^{10}Be concentration ratios have been explained in previous studies by invoking geological processes (Balco et al., 2019; Rand and Goehring, 2019). First, we examine the Notebook Cliffs, Turtle Rock, and scoria cone sites (see Figs. S1–S5 in the Supplement) to determine if localised glacial-geological changes at Mt Murphy permit the existence of paired in situ ^{14}C–^{10}Be discordant exposure ages at the same elevation as paired in situ ^{14}C–^{10}Be concordant exposure ages. A USGS trimetrogon aerial (TMA) photograph shows that in 1966, in contrast to today, the lower scoria cone outcrop was almost completely buried by ice (see Fig. S7 of Nichols et al., 2024). This finding indicates that samples CIN-112 and CIN-108 were shielded by ice for a non-zero time between 6.4 ka and present (Adams et al., 2022; Balco et al., 2023). A discordant initial in situ ^{14}C age for CIN-112 (3.4 ± 0.3 ka, 179 m a.s.l.) that is younger than the ^{10}Be exposure age (6.6 ± 0.4) from the same sample and other in situ ^{14}C ages from higher elevation scoria cone samples supports the interpretation that such burial occurred during the late Holocene. The in situ ^{14}C replicate measurement, CIN-112-R, however, yielded an exposure age of 7.2 ± 0.9 ka, which is in agreement with the corresponding ^{10}Be age. Both in situ ^{14}C exposure ages determined from measurements of sample CIN-108 (collected from the same outcrop and elevation as CIN-112) are early-mid Holocene (CIN-108 – 6.3 ± 0.7 ka; CIN-108-R – 7.8 ± 1.0 ka). With the exception of the initial ^{14}C exposure age from sample CIN-112, all exposure ages from the lower scoria cone outcrop (Adams et al., 2022) suggest that ice cover during the late Holocene was short-lived.

At both Turtle Rock and Notebook Cliffs, there is little evidence to suggest prolonged cover or burial of samples. At Turtle Rock, discordant in situ ^{14}C–^{10}Be exposure ages of TUR-117 and TUR-123 could be due to individual samples being partially shielded by till or ice debris cover during the Holocene, but the preferential sampling of topographic highs makes this less likely (Johnson et al., 2020). Furthermore, the in situ ^{14}C exposure age of TUR-117-R (8.2 ± 1.1 ka) agrees with the sample's existing ^{10}Be exposure age. There is no geological explanation for measurements of the same nuclide (in situ ^{14}C) on the same two samples (TUR-117, CIN-112) yielding different exposure ages. At Notebook Cliffs, all in situ ^{14}C exposure ages ($n = 3$) are late Holocene and discordant with existing ^{10}Be ages, implying inheritance in ^{10}Be and prolonged burial of all three samples. The three Notebook Cliffs in situ ^{14}C exposure ages contradict evidence from lower elevations of Mt Murphy that indicate early to mid-Holocene deglaciation from 9–6 ka (Adams et al., 2022; Balco et al., 2023; Johnson et al., 2020). In situ ^{14}C ages from Notebook Cliffs could be reconciled with the currently accepted Mt Murphy deglaciation history if a localised ice dome had persisted atop Notebook Cliffs, shielding samples until the late Holocene. The flat top of the Notebook Cliffs site would favour persistence of a post-glacial ice dome; however, there is no physical evidence for this having occurred (Johnson et al., 2020)

Except for late Holocene ice cover of samples CIN-108 and CIN-112 at the lower scoria cone outcrop, evidence for localised geological and topographical drivers of repeated burial and exposure of samples at Mt Murphy are lacking. Instead, differing exposure and transport histories of erratics prior to deposition might explain the concordant and discordant paired ^{14}C–^{10}Be ages observed at the same elevation at Mt Murphy. A similar mechanism, whereby some erratics are initially exposed at higher elevation (and thus subjected to a higher nuclide production rate) has been used to explain the presence of concordant older ^{14}C–^{10}Be ages and discordant young ^{14}C ages at comparable elevations at another site, Shark Fin Nunatak, adjacent to Tucker Glacier in the Ross Sea Embayment (Balco et al., 2019). This hypothesis is supported by both extensive weathering of older samples at Shark Fin Nunatak, and the presence of cliffs of the same lithology upstream, from which erratics could have originated (Balco et al., 2019). However, exposed outcrops with lithologies matching the aplite, granite, and gneiss lithologies of erratics observed at Mt Murphy and surrounding nunataks (Adams et al., 2022; Johnson et al., 2020) are absent in the near vicinity. The nearest outcrop upstream, Mt Takahe (Figs. S6 and S7a in the Supplement) $\sim$ 100 km to the south, is composed of mafic extrusive rock (Ohio State Polar Rock Repository; https://prr.osu.edu/collection/, last access: 15 February 2024). Such prior exposure and transport of erratics from nunataks with the same lithologies as those found at Mt Murphy would necessitate dramatic past ice flow reorganization, for which there is no evidence (see Supplement S1 and Figs. S6–S8 in the Supplement).

4.3.1 Identifying sites with paired ^{14}C–^{10}Be nuclide systematics resembling those of Mt Murphy samples

Paired ^{14}C–^{10}Be nuclide ratios measured in samples from Shark Fin Nunatak all indicate a simple exposure history (Table 4 and Sect. S5 – Site 4 in the Supplement), which contrasts with paired ^{14}C–^{10}Be nuclide ratios obtained from Mt Murphy. The sites at Mt Murphy instead exhibit a mixture of Type 1 (simple), Type 2 (complex), and a few borderline Type 3 (impermissible) exposure histories (see Figs. 2 and

4). To determine if any other sites in Antarctica, or elsewhere, display similar paired ^{14}C–^{10}Be nuclide diagram systematics to Mt Murphy, we used an SQL search filter implemented in MATLAB (Balco, 2020b) to extract from the informal online database ICE-D (https://version2.ice-d.org/antarctica/, last access: 29 March 2024) sites with ^{14}C–^{10}Be exposure age pairs that meet the following criteria: (1) the ratio of the ^{10}Be exposure age to the ^{14}C exposure age is $< 4:1$ and (2) the ^{10}Be apparent exposure age is < 11.7 ka (indicating the sample was exposed during the Holocene). We applied these filters to remove ^{10}Be apparent exposure ages older than the Holocene because ^{10}Be inheritance and its impact on measurement accuracy is well-documented, especially in Antarctica, where limited erosion often results in ^{10}Be nuclide inventories which encapsulate more than one glacial cycle. A summary of all sites with paired in situ ^{14}C–^{10}Be exposure ages compiled from ICE-D that satisfy our search criteria ($n = 29$) is provided in Table 4 and numbered in Fig. 1. Age-elevation plots and paired nuclide diagrams for samples from each site can be found in Supplement S5.

An examination of the paired ^{14}C–^{10}Be nuclide diagrams from the twenty-nine sites returned from our search of the ICE-D database which includes data from Mt Murphy (Table 4) indicate samples that exhibit paired ^{14}C–^{10}Be concentrations consistent with a Type 1 simple exposure history are the most prevalent at over half of sites ($n = 15$), e.g., Kangiata Nunata Sermia, Greenland (Young et al., 2021; Fig. 6b). There are two sites where samples exhibiting a Type 2 complex exposure history are dominant, including Rhône Glacier forefield in the European Alps (Goehring et al., 2011, Fig. 6c). A total of six sites exhibit Type 3 ^{14}C–^{10}Be ratios (indicative of impermissible exposure histories), but many of these datasets contain just one sample. An exception is Sjögren Glacier (Figs. 6d and 7) on the Antarctic Peninsula where numerous samples exhibit impermissible ^{14}C–^{10}Be nuclide ratios (Balco and Schaefer, 2013). Notably only scoria cone, Turtle Rock and Mt Hope, Beardmore Glacier (Site 9) display an equal distribution of both simple (Type 1) and complex (Type 2) exposure histories. An interrogation of the geologic setting of these endmember sites, which consist of multiple samples of the same type, did not provide information that could help explain the concordant and discordant exposure ages or the mixture of Type 1, Type 2 and borderline Type 3 paired ^{14}C–^{10}Be nuclide ratios at Mt Murphy (Fig. 6a). For a detailed account of our geological interrogation and comparison of endmember sites to the Mt Murphy dataset, see Sect. S1.2 in the Supplement.

The impermissible (Type 3) paired nuclide ^{14}C–^{10}Be ratios from Sjögren Glacier (Site 12 in Table 4) present an opportunity to attempt to identify the cause of high in situ ^{14}C–^{10}Be ratios such as those observed in samples CIN-108-R (Fig. 4). As well as several replicate in situ ^{14}C measurements having been made on samples from there, Sjögren Glacier Site C bears a close geomorphic resemblance to the scoria cone site at Mt Murphy making it a useful comparison with our dataset. To investigate possible causes of borderline Type 3 ratios at Mt Murphy, we modelled scenarios where samples from Sjögren Glacier were subject to either rapid exhumation from ice (Fig. 7a) or prolonged burial under ice (Fig. 7b), both of which would lead to higher in situ ^{14}C production relative to ^{10}Be production in the subsurface (see Sect. 1.1). In these scenarios, in situ ^{14}C nuclide concentration is therefore expected to increase relative to ^{10}Be and may explain impermissible Type 3 ^{14}C–^{10}Be concentration ratios. However, we observed ratios of in situ ^{14}C–^{10}Be relative to ^{10}Be concentrations at Sjögren Glacier that cannot be reconciled by either of these processes. In both scenarios, if the concentration of ^{10}Be atoms is < 2000 at g^{-1}, which is very low, we observe high modelled ^{14}C–^{10}Be ratios comparable to the in situ ^{14}C–^{10}Be concentration ratios in Sjögren Glacier samples. However, as soon as ^{10}Be nuclide concentrations exceed 1000–2000 at g^{-1}, we no longer observe high ^{14}C–^{10}Be ratios due to high erosion rates rapidly removing accumulated nuclides or faster decay of in situ ^{14}C relative to ^{10}Be offsetting the higher ^{14}C–^{10}Be subsurface production ratio. In addition, all measured in situ ^{14}C nuclide concentrations from Sjögren Glacier Site C appear to be systematically offset by approximately 5000 extra ^{14}C atoms, suggesting a potential source of contaminant in situ ^{14}C. A high proportion of those samples consist of vein quartz (see Table S3), and it is possible that impermissible (Type 3) ^{14}C–^{10}Be ratios observed at Sjögren Glacier are due to an additional carbon source present in the quartz or incorporated during in situ ^{14}C extraction instead of being geologically caused (Nichols and Goehring, 2019).

Overall, neither our comparison of the geomorphic setting of the Mt Murphy site with other locations (Sect. 4.1 and Supplement 1), our interrogation of paired ^{14}C–^{10}Be ratios from the ICE-D database (including those from sites with Holocene ^{14}C–^{10}Be exposure ages), nor our efforts to model seemingly impermissible high ^{14}C–^{10}Be concentration ratios (Sects. 4.3 and S1.3) could provide a plausible geological explanation for the in situ ^{14}C–^{10}Be dataset from Mt Murphy. In contrast, the sensitivity analysis of the Mt Murphy data (Sect. 4.2) did improve reproducibility of the older in situ ^{14}C exposure ages, suggesting that the explanation for the young discordant in situ ^{14}C ages is likely related to sample preparation.

4.4 In situ ^{14}C reproducibility assessment

To investigate potential sources of sample preparation uncertainty, we focus on evaluating in situ ^{14}C measurement reproducibility using both our new data from Mt Murphy and existing datasets from the ICE-D database for samples where two or more measurements had been made, excluding measurements of laboratory intercomparison materials such as CRONUS-A. In addition to the Mt Murphy results, a further 25 samples with repeat in situ ^{14}C measurements are available in ICE-D, and we present a further two

https://doi.org/10.5194/gchron-8-255-2026

Table 4. Full list of paired in situ ^{14}C–^{10}Be surface exposure ages extracted from ICE-D, as described in the text. Paired nuclide ratio type refers to the dominant position of paired ^{14}C–^{10}Be ratio ellipses on a paired nuclide diagram (Fig. 2). Paired nuclide diagrams from each site are listed as the dominant type(s), with instances of the less common types denoted in brackets. Abbreviations for AMS and in situ ^{14}C extraction laboratories are as follows: CEREGE (Centre Européen de Recherche et d'Enseignement des Géosciences de l'Environnement), France; ETH Zurich (Swiss Federal Institute of Technology in Zurich), Switzerland; KIST (Korean Institute of Science and Technology), South Korea; LDEO (Lamont-Doherty Earth Observatory), USA; LLNL (Lawrence Livermore National Laboratory), USA; NOSAMS (National Ocean Sciences Accelerator Mass Spectrometry Laboratory at the Woods Hole Oceanographic Institution), USA; and SUERC (Scottish Universities Environmental Research Centre), UK. Shark Fin nunatak ^{10}Be ages are > 11.7 ka, so do not meet one of our search criteria, but those samples are included here due to their similarities in age versus elevation profile to Mt Murphy. Note in the "^{14}C–^{10}Be Ratio Type" column the most prevalent ^{14}C–^{10}Be ratio observed in samples from that site is indicated first and unbracketed, e.g. 1, and if the site also exhibits a minority of a different type the minority is indicated in brackets, e.g. 1(2).

Location ID	Short Name (ICE-D)	Site Name, Location	^{14}C–^{10}Be ratio type	In situ ^{14}C extraction lab	^{14}C AMS lab	Reference ^{10}Be dataset	Reference in situ ^{14}C dataset
1	REA	Mt.Rea, Sarnoff Mts.	3	Tulane CNL	NOSAMS	Stone et al. (2003)	ICE-D*
2	TR	Turtle Rock, Mt Murphy	1 2 (3)	Tulane CNL	NOSAMS	Johnson et al. (2020)	This paper
3	NMAS	North Masson Range, Framnes Mts.	3 (1)	SUERC	SUERC	Mackintosh et al. (2007)	White et al. (2011)
4	SKF	Sharkfin nunatak, Tucker Gl.	1 (2)	Tulane CNL	LLNL	Balco et al. (2019)	Balco et al. (2019)
5	MZS	Mario Zuchelli Station, Terra Nova Bay	1	Tulane CNL	LLNL	Goehring et al. (2019b)	Goehring et al. (2019b)
6	WHITS	Mt. Whitmore, Whitmore Mts.	N/A	Tulane CNL	NOSAMS	Spector et al. (2019)	Spector et al. (2019)
7	KAYCONE	scoria cone, Mt Murphy	1 2	Tulane CNL	NOSAMS	Adams et al. (2022)	This paper
8	NOTE	Notebook Cliffs, Mt Murphy	2	Tulane CNL	NOSAMS	Johnson et al. (2020)	This paper
9	HOPE	Mt. Hope, Beardmore Glacier	1 2	Tulane CNL	NOSAMS	Spector et al. (2017)	ICE-D*
10	CMARSH	Cape Marsh, Robertson Island	1	KIST	KIST	Jeong et al. (2018)	Jeong et al. (2018)
11	FRAMNES	Cape Framnes, Jason Peninsula	1 (2)	KIST	KIST	Jeong et al. (2018)	Jeong et al. (2018)
12	SJOC	Site C, Sjögren Glacier	3	Tulane CNL	NOSAMS	Balco and Schaefer (2013)	ICE-D*
13	DRYE	Site E, Drygalski Glacier	1 3 (2)	Tulane CNL	NOSAMS	Balco and Schaefer (2013)	ICE-D*
14	KRING	Mt. Kring, David Glacier	3	Tulane CNL	NOSAMS	Stutz et al. (2021)	ICE-D*
15	DIAMOND	Diamond Hill, Darwin-Hatherton Glaciers	3	Tulane CNL	NOSAMS	Hillebrand et al. (2021)	Hillebrand et al. (2021)
16	DANPB1	Danum Platform, Darwin-Hatherton Glaciers	1 (3)	Tulane CNL	NOSAMS	Hillebrand et al. (2021)	Hillebrand et al. (2021)
17	Goeh2011-A	Rhône Glacier, Swiss Alps	2	LDEO	Uni of Arizona	Goehring et al. (2011)	Goehring et al. (2011)
18	Hipp2014-A	Gotthard Pass, Swiss Alps	1	ETH Zurich	ETH Zurich	Hippe et al. (2014)	Hippe et al. (2014)
19	KBR1	KNS bedrock 1, Kangiata Nunata Sermia	1	LDEO	CEREGE	Young et al. (2021)	Young et al. (2021)
20	KBR2	KNS bedrock 2, Kangiata Nunata Sermia	1	LDEO	CEREGE	Young et al. (2021)	Young et al. (2021)
21	INGLE1	Outboard ice margin, Inglefield Land	1	ETH Zurich	ETH Zurich	Søndergaard et al. (2020)	Søndergaard et al. (2020)
22	MACAULAY	Macaulay Boulder Field, Southern Alps	1 (3)	LDEO	LLNL-CAMS	Putnam et al. (2010)	Schimmelpfennig et al. (2012)
23	MARRAIT	Marrait Moraine, Jakobshavn Isfjord	1	LDEO	LLNL-CAMS	Young et al. (2013)	Young et al. (2014)
24	GHm-Out5	Grey Hunter massif, MacArthur Mts., Yukon	1	Tulane CNL	NOSAMS	Goehring et al. (2022)	Goehring et al. (2022)
25	SISPEN-W	Sisimiut Peninsula, Kangerlassuaq	1	LDEO	CEREGE	Sbarra et al. (2022)	Sbarra et al. (2022)
26	Mammoth-Forefield	Mammoth Gl., Wind River Range, WY	1	Tulane CNL	NOSAMS	Jones et al. (2023)	Jones et al. (2023)
27	Conness-Forefield	Conness Gl., Sierra Nevada, CA	N/A	Tulane CNL	NOSAMS	Jones et al. (2023)	Jones et al. (2023)
28	JIF-Forefield	Juneau Ice Field, Coast Mts., AK	1 3	Tulane CNL	NOSAMS	Jones et al. (2023)	Jones et al. (2023)
29	N/A	Engabreen Glacier, Norway#	3	Tulane CNL	NOSAMS	Rand and Goehring (2019)	Rand and Goehring (2019)

Engabreen glacier paired in situ ^{14}C–^{10}Be data are not archived in ICE-D but are included to demonstrate a geological solution to a "Type 3" dataset.

* Unpublished in situ ^{14}C data; these data are freely available in ICE-D under the public release requirements of the National Science Foundation (NSF) U.S. Antarctic Program.

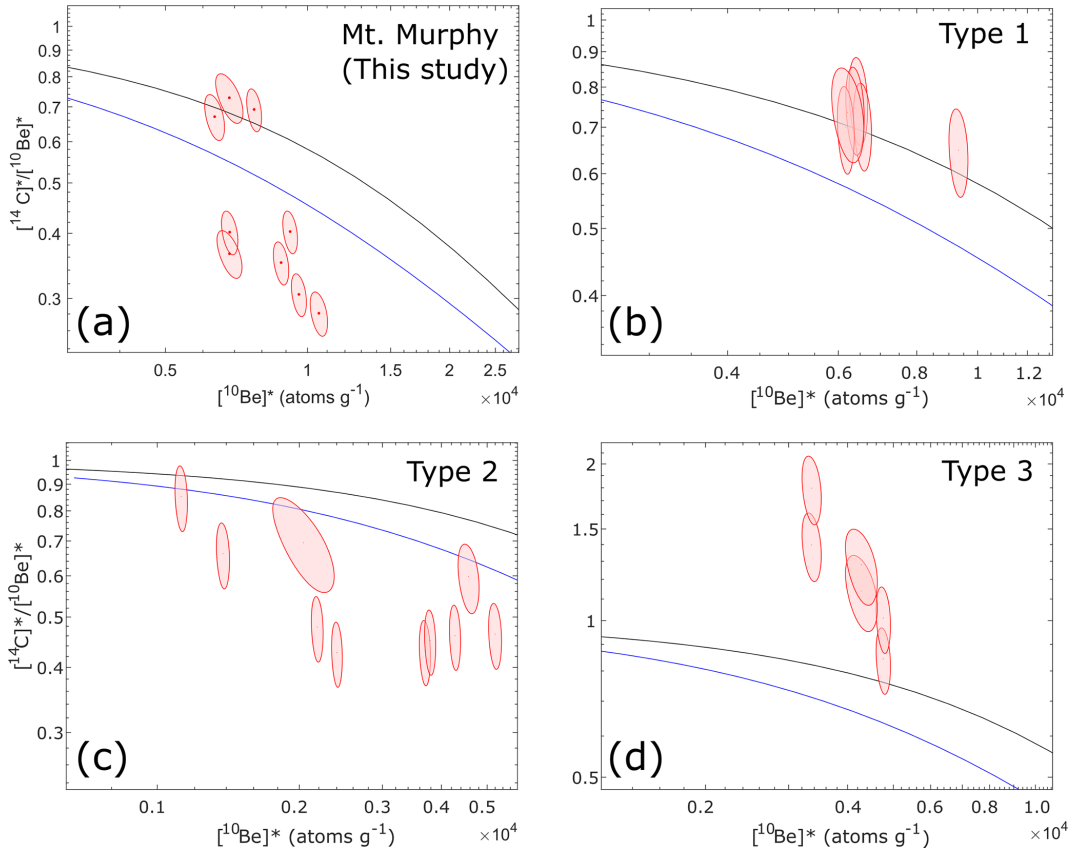

Figure 6. Paired in situ ^{14}C–^{10}Be nuclide concentrations from **(a)** Mount Murphy (this study), and paired ^{14}C–^{10}Be concentration data from other sites extracted from ICE-D including: **(b)** Kangiata Nunata Sermia (KNS), Greenland (Type 1, dominated by concordant ages), **(c)** Rhône Glacier, Switzerland, (Type 2, complex exposure – burial history) and **(d)** Sjögren Glacier, Antarctic Peninsula (Type 3 – impermissible exposure history-dominated dataset). NB: Other paired ^{14}C–^{10}Be datasets classified using the same system are displayed in Table 4. All paired ^{14}C–^{10}Be concentration ratios are normalised to the sample-specific production rate using the LSDn scaling scheme and plotted as ellipses at 68 % confidence (Lifton et al., 2014) using the CRONUS-Earth calibration dataset for ^{10}Be (Borchers et al., 2016) and measurements of CRONUS-A at Tulane University for in situ ^{14}C (Goehring et al., 2019a). Note different in situ ^{14}C production rate calibration datasets would be more suitable for generating paired nuclide diagrams presented in panel **(b)** (Young et al., 2014) and panel **(c)** (Goehring et al., 2011), but do not change the type classification for each dataset. For further information on paired nuclide diagrams and type classification scheme, see Sect. 1.2.

samples with replicate in situ ^{14}C measurements from the Leymon High Core (Lupker et al., 2015) bringing the total number of samples with replicate in situ ^{14}C measurements to 31. The majority of replicate measurements are reported from samples sourced from the Antarctic Peninsula (Balco and Schaefer, 2013), Weddell Sea Embayment (Nichols et al., 2019), Promontory Point (Pleistocene Lake Bonneville), Utah (Lifton et al., 2015a), and the Northwest Highlands, Scotland (Borchers et al., 2016). To each in situ ^{14}C concentration, we assign a measurement uncertainty of 6 % of the total concentration reported from AMS measurements for each replicate. Using a 6 % uncertainty is appropriate here because the majority of replicate measurements presently in the ICE-D database were measured at Tulane and 6 % is the published, and conventionally used, measurement uncertainty from that laboratory based on reproducibility of in situ ^{14}C measured in CRONUS-A from 2015–2018 (Goehring et al., 2019a) cited in numerous studies (e.g., Balco et al., 2019, Nichols et al., 2019, Rand et al., 2025). In cases where in situ ^{14}C replicates were reported from a different extraction laboratory, and that laboratory reports measurement uncertainty exceeding 6 %, we assign the larger value to each in situ ^{14}C concentration.

From our reproducibility assessment of 31 replicate samples, 18 display one or more in situ ^{14}C measurements that do not replicate within 6 % (1σ) measurement uncertainty (Fig. 8). There is a slight increase in reproducibility at 2σ, but 15 samples still exhibit one or more in situ ^{14}C measurements that are not reproducible (Fig. S13 in the Supplement). These results include the 3 out of 4 in situ ^{14}C concentrations reported from Mt Murphy which do not replicate within the 6 % (1σ) measurement uncertainty, and 2 of 4 in situ ^{14}C

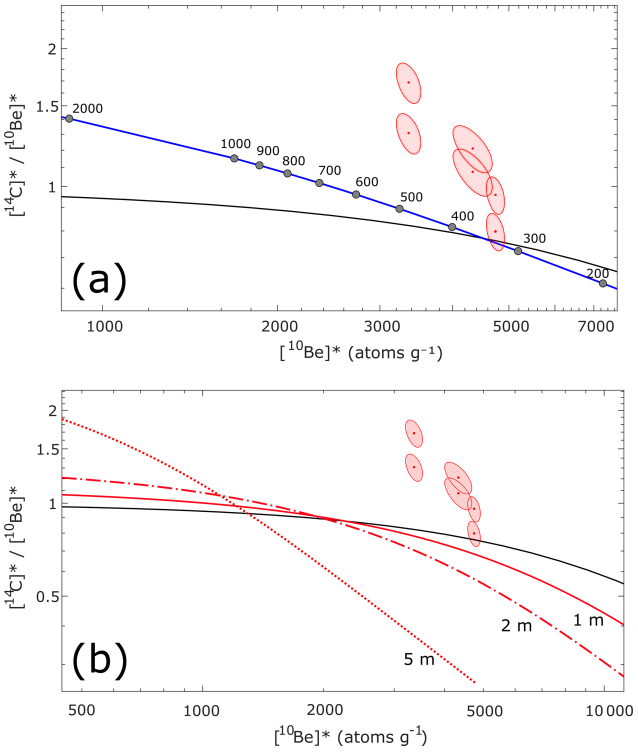

Figure 7. Plots showing modelled subsurface production scenarios that lead to a higher in situ ^{14}C relative to ^{10}Be ratio than typical for the surface. Panel **(a)** shows in situ ^{14}C–^{10}Be nuclide ratios as a function of glacial exhumation rate integrated over a time t, assuming both ^{10}Be and in situ ^{14}C nuclide concentrations are zero at the LGM ($t = 20\,000$ years). The black line represents the constant exposure line and blue line the steady erosion line including muon production. Grey dots indicate modelled in situ ^{14}C–^{10}Be nuclide concentration ratios for an erosion rate which is specified above each dot (mm kyr^{-1}). Panel **(b)** shows modelled in situ ^{14}C–^{10}Be nuclide concentrations as a function of burial under different ice thicknesses over Holocene timescales (plotted as isolines). The black line represents the constant exposure line, but we omit the steady erosion line to improve legibility. On both plots red ellipses indicate in situ ^{14}C–^{10}Be concentration ratios measured in samples from Sjögren Glacier, Site C (68 % confidence). Plots are generated using the surface and subsurface production rate estimating code from (Balco et al., 2023).

concentrations do not replicate at 2σ (see Sect. 3.1). Notably, replicate measurements included in our Holocene filter analysis from the Antarctic Peninsula (Sjögren and Drygalski Glaciers, $n = 5$; see Sect. 4.3.1 and Fig. 8) also yielded many impermissible paired ^{14}C–^{10}Be ratios, suggesting a possible link between in situ ^{14}C reproducibility and Type 3 ^{14}C–^{10}Be concentration ratios. However, the lack of an apparent geologic explanation for irreproducibility of in situ ^{14}C measurements from field samples (see Sect. 4.3) suggests that the assumed measurement uncertainty may be too low. Such an issue has been noted previously by Borchers et al. (2016) where scatter of in situ ^{14}C concentrations from calibration sites (including the Northwest Highlands) exceeded stated measurement uncertainties.

4.4.1 In situ ^{14}C reproducibility – CRONUS-A and blank data

The long-term average in situ ^{14}C concentration measured in CRONUS-A reported from different in situ ^{14}C extraction facilities ranges from $6.12 \pm 0.32 \times 10^5$ at g^{-1} for Tulane CNL to $7.28 \pm 0.03 \times 10^5$ at g^{-1} at ETH Zurich (Lupker et al., 2019). The CRONUS-A value reported from Tulane CNL, $6.12 \pm 0.32 \times 10^5$ at g^{-1} (Goehring et al., 2019a), is 5 %–10 % lower than other in situ ^{14}C extraction laboratories and below the consensus interlaboratory value ($n = 23$) of 6.97×10^5 at g^{-1} of (Jull et al., 2015). In addition, the long-term CRONUS-A value suggested by all CRONUS-A measurements reported from Tulane CNL is even lower; $5.88 \pm 0.59 \times 10^5$ at g^{-1} ($n = 18$) from 22 December 2016–12 March 2021 (Table S5, Balco et al., 2023). LDEO report a higher than average – and 15.8 % higher than Tulane CNL – value for CRONUS-A ($n = 13$) of $6.98 \pm 0.25 \times 10^5$ at g^{-1} for graphitised samples (Lamp et al., 2019; Young et al., 2021). Interlaboratory comparison of CRONUS-A in situ ^{14}C values, therefore, is consistent with findings from our within laboratory sensitivity tests in Sect. 4.2 that suggest a 6 % in situ ^{14}C measurement uncertainty is too low (Jull et al., 2015).

Inconsistencies in the interlaboratory reproducibility of CRONUS-A and corresponding underestimation of in situ ^{14}C measurement uncertainty have been documented in previous studies. These highlight that laboratories uniformly underestimated the magnitude by which empirical coefficients of variation exceeded average reported analytical uncertainties for all nuclides (Jull et al., 2015; Phillips et al., 2016a). However, the underestimation in the reported analytical uncertainty exceeds 300 % for ^{14}C on the CRONUS-A material (Phillips et al., 2016b), although subsequent analyses of CRONUS-A reproducibility following the CRONUS-Earth Project (e.g., Fülöp et al., 2019b; Goehring et al., 2019a; Lamp et al., 2019; Lifton et al., 2023) may alter this value.

The CRONUS-A intercomparison material is derived from a high elevation site (1612 m) in Antarctica with millions of years of constant exposure, making it saturated with respect to ^{14}C (mean value $= 6.93 \pm 0.44 \times 10^5$ at g^{-1}, Jull et al., 2015). Reproducibility estimates from CRONUS-A are, therefore, only representative for high concentration samples, for which AMS counting errors and blank contributions are typically low (Hippe, 2017). Achieving the same level of measurement precision in a sample with a lower concentration of in situ ^{14}C is more challenging, and a typical sample exposed during the Holocene will yield an in situ ^{14}C concentration lower than CRONUS-A. For instance, sample TUR-132 from Turtle Rock (7.4 ± 1.2 ka, 446 m a.s.l.) has a mean in situ ^{14}C concentration of $1.32 \pm 0.08 \times 10^5$ at g^{-1} ($n = 2$). Samples exposed during the Holocene, and particu-

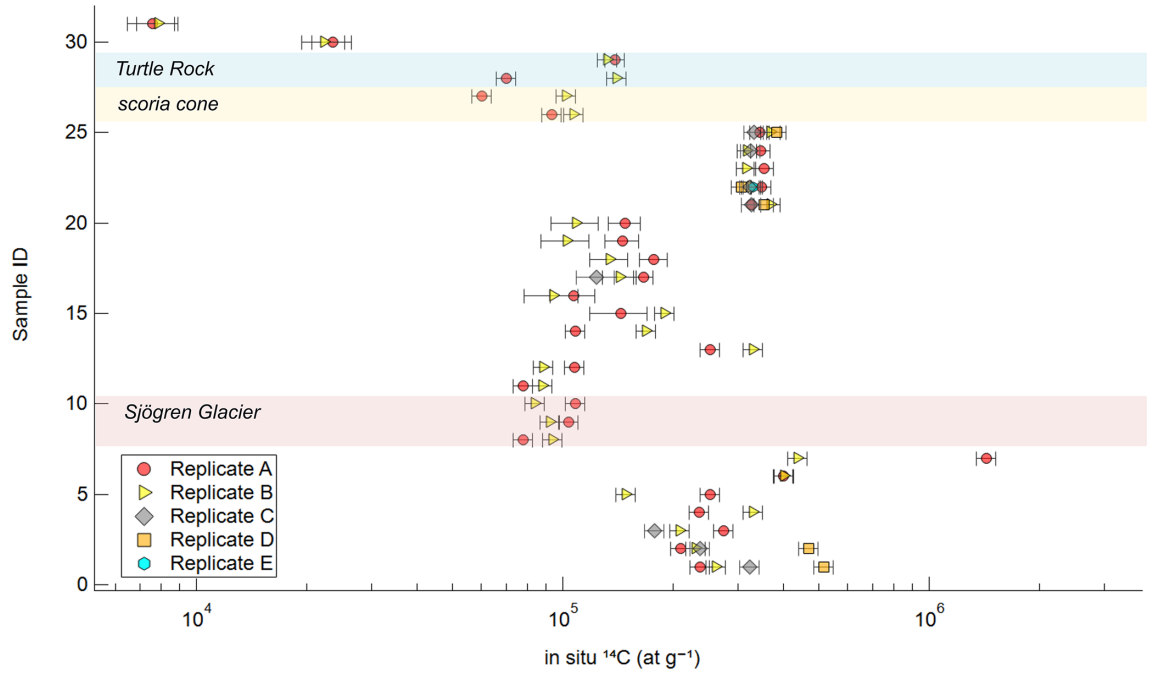

Figure 8. In situ ^{14}C concentrations in ICE-D with one or more replicate measurements from the same sample ($n = 31$). To enable comparison with the Mt Murphy dataset, in situ ^{14}C concentration error bars represent a 6 % measurement uncertainty based on repeatability of CRONUS-A measured at Tulane CNL (Goehring et al., 2019a). The graph displays all samples with repeat in situ ^{14}C concentrations uploaded to ICE-D as of 29 March 2024 as well as repeat in situ ^{14}C measurements from Mt Murphy samples (this study) and Leymon High bedrock core samples (Lupker et al., 2015). We use the measurement uncertainty reported with a particular study when this value exceeds the nominal 6 % (1σ) uncertainty. Replicate in situ ^{14}C measurements discussed in the text, including Turtle Rock, scoria cone, and Sjögren Glacier, are indicated by shaded bars. See Table S3 for full list of sample details.

Table 5. Summary of CRONUS-A intercomparison material and long-term blank values reported from different in situ ^{14}C extraction facilities. Note: Tulane CNL and LDEO are examined more closely over several measurement cycles because in situ ^{14}C measured from Mt Murphy samples was extracted at both facilities. The latest AixMICADAS gas ion source AMS measurements reported by LDEO highlight how gas ion source AMS in situ ^{14}C measurements have reduced ^{14}C background levels reported by LDEO by removing a potential source of ^{14}C contamination from graphitisation.

Extraction Laboratory	CRONUS A (at g^{-1})	No. CRONUS-A	Representative blank (atoms)	Associated Publication
Tulane – reported 2019	$6.12 \pm 0.32 \times 10^5$	10	$0.98 \pm 0.32 \times 10^5$	Goehring et al. (2019a)
Tulane – Mt Murphy (initial)	$5.88 \pm 0.59 \times 10^5$	18	$4.53 \pm 0.24 \times 10^4$	*Balco et al. (2023)
Tulane – Mt Murphy (replicates)	$7.11 \pm 0.10 \times 10^5$	1	$7.14 \pm 0.30 \times 10^4$	This publication.
LDEO – Graphitised pre-2014	$6.74 \pm 0.10 \times 10^5$	5	$1.19 \pm 0.37 \times 10^5$	Lamp et al. (2019)
LDEO – Graphitised post-2014	$6.98 \pm 0.25 \times 10^5$	13	$1.17 \pm 0.37 \times 10^5$	Young et al. (2021)
LDEO – AixMICADAS	$6.62 \pm 0.10 \times 10^5$	5	$8.84 \pm 1.21 \times 10^4$	Young et al. (2021)
ETH Zurich (2011–2013)	$7.09 \pm 0.39 \times 10^5$	13	$3.48 \pm 2.04 \times 10^4$	Lupker et al. (2015)
ETH Zurich 2018	$7.28 \pm 0.03 \times 10^5$	7	$2.63 \pm 1.05 \times 10^5$	Lupker et al. (2019)
Cologne	$6.72 \pm 0.71 \times 10^5$	6	$1.00 \pm 0.68 \times 10^4$	Fülöp et al. (2015)
ANSTO	$6.93 \pm 0.44 \times 10^5$	14	$0.98 \pm 0.68 \times 10^4$	Fülöp et al. (2019)
PRIME Lab (Purdue)	$6.89 \pm 0.04 \times 10^5$	6	$1.84 \pm 0.38 \times 10^5$	Lifton et al. (2015b)
PRIME Lab (Purdue)	$7.08 \pm 0.17 \times 10^5$	12	$3.40 \pm 0.90 \times 10^4$	Lifton et al. (2023)
Working interlaboratory – Mean	$6.93 \pm 0.44 \times 10^5$	23		Jull et al. (2015)
Working interlaboratory – Median	6.97×10^5	23		Jull et al. (2015)

* In Balco et al. (2023), long-term blank values for Tulane CNL surface sample measurements presented in our present study are not reported, but blank variability at Tulane CNL spanning the same time period is discussed at length.

larly those at low elevations such as the scoria cone and Kay Peak, are therefore more sensitive than CRONUS-A to blank correction.

For our samples, the blank correction reported from Tulane CNL for in situ ^{14}C repeat measurements was higher than that of the initial ^{14}C measurements (Table 5). The differences in in situ ^{14}C concentrations may be explained, in part, by several changes made to the extraction line at Tulane CNL between the two sets of extractions, including the addition of a new coil trap (Lifton et al., 2023) and a new mullite tube which was previously observed to increase background ^{14}C (see Methods, Sect. 2.2). However, our sensitivity analyses indicate that applying different blank corrections based on the long-term blank data from Tulane CNL (cf. Table S5, Balco et al., 2023) neither reconcile young initial in situ ^{14}C ages with discordant ^{10}Be ages or older replicate in situ ^{14}C ages (see Sect. 4.2) nor the in situ ^{14}C concentrations from our Mt Murphy dataset that do not reproduce.

In an additional effort to identify a potential cause for lack of in situ ^{14}C reproducibility, we investigated if heterogeneities in quartz mineral separates could yield notably different in situ ^{14}C concentrations in the same sample (see Sect. S4, Tables S7 and Table S8 in the Supplement). Impurities in quartz mineral separates have previously been evidenced to negatively impact the reproducibility of ^{10}Be (Corbett et al., 2022). However, we found no link between abundance of impurities in quartz mineral separates and in situ ^{14}C reproducibility in the Mt Murphy samples.

4.5 Summary and suggestions for future work

The findings presented in this paper suggest that routine laboratory uncertainties reported with our samples from Mt Murphy likely underestimated the true measurement uncertainty of in situ ^{14}C for our dataset. This result is consistent with previous findings from the CRONUS-Earth Project (Borchers et al., 2016; Phillips et al., 2016a) and other studies (Hippe, 2017; Jull et al., 2015) where issues regarding the interlaboratory variation in reported CRONUS-A in situ ^{14}C concentrations ($\sim 15\,\%$) and in situ ^{14}C blank variability were shown to impact the accuracy and precision of in situ ^{14}C measurements. A seemingly isolated issue associated with the initial in situ ^{14}C extractions likely resulted in systematically young ages inconsistent with both the replicate measurements and previously published ^{10}Be exposure ages from Mt Murphy, as well as with records of the deglacial history of the Amundsen Sea Embayment more widely. The nature of the apparent loss of in situ ^{14}C from most of our samples during the initial extractions is not understood and is atypical of the considerable number of in situ ^{14}C measurements reported from Tulane CNL. Nevertheless, complexities in our dataset highlight the value of routinely conducting replicate analyses not just for in situ ^{14}C, but for all cosmogenic nuclides, especially if a dataset displays systematic offsets that cannot be accounted for by reported uncertainties. Ongoing developments, including automation of in situ ^{14}C extraction (Goehring et al., 2019a; Lifton et al., 2023; Lupker et al., 2019), will help facilitate analysis of the additional replicates and process blanks needed to improve the precision of in situ ^{14}C measurements. With a focus on improving in situ ^{14}C analytical reproducibility and precision, we therefore make the following suggestions for future work, which will ultimately contribute to the provision of robust combined ^{14}C–^{10}Be chronologies:

- Routinely undertake and report more in situ ^{14}C replicate measurements. This will provide a check on quality control.
- Conduct an in situ ^{14}C interlaboratory comparison study using additional intercomparison materials (e.g., CoQtz-N, CRONUS-R) to determine if apparent interlaboratory offsets reported for in situ ^{14}C measurements of CRONUS-A are specific to CRONUS-A or are replicated for other samples. If interlaboratory offsets for in situ ^{14}C measurements of CRONUS-A are consistent across other intercomparison materials, a standardization consensus value can be established, facilitating comparison of exposure age data generated by different in situ ^{14}C extraction facilities.

5 Conclusion

In this study, we presented new in situ ^{14}C ages from Mt Murphy, West Antarctica and compared them with published ^{10}Be ages, identifying numerous conflicting exposure histories. Young in situ ^{14}C ages from high elevations that are discordant with ^{10}Be measured in the same sample appear to have deglaciated after concordant paired ^{14}C–^{10}Be exposure ages from lower elevations with simple exposure histories. There is no plausible geological explanation for divergent concordant-discordant exposure histories or excess scatter observed within the in situ ^{14}C dataset. Instead, we find that most of the replicate in situ ^{14}C measurements performed on samples from Mt Murphy do not reproduce within a $6\,\%$ 1σ internal measurement uncertainty. Furthermore, concordant ^{14}C–^{10}Be pairs at Mt Murphy with simple exposure histories exhibit reproducible in situ ^{14}C concentrations, but discordant in situ ^{14}C exposure ages suggestive of complex exposure are not reproducible. A subsequent sensitivity analysis applying a larger non-standard $10\,\%$ uncertainty to in situ ^{14}C concentrations improved the reproducibility of one of the replicate in situ ^{14}C measurements; however, despite the larger assigned measurement uncertainty, half the in situ ^{14}C concentrations still did not reproduce. These observations from Mt Murphy are reflected in archived in situ ^{14}C concentrations extracted from the informal cosmogenic-nuclide exposure-age database (ICE-D), where replicate concentrations measured in 18 of 31 samples fail to reproduce within the $6\,\%$ 1σ measurement uncertainty (15 of 31 at 2σ).

In summary, the results of our analysis of in situ ^{14}C–^{10}Be exposure ages from ICE-D are consistent with the interpretation that discordant in situ ^{14}C–^{10}Be exposure ages from Mt Murphy are a result of isolated issues with in situ ^{14}C reproducibility at the Tulane Cosmogenic Nuclide Laboratory (Tulane CNL), while concordant ^{14}C–^{10}Be pairs are consistent with deglaciation (between 9–6 ka) identified by previous studies. Tulane CNL has produced a comparatively large number of in situ ^{14}C replicate measurements; having access to this laboratory's quality control data enabled us to identify inconsistencies in our dataset that crucially prevented us from drawing incorrect conclusions regarding Mt Murphy's deglacial history. We attribute the new discordant in situ ^{14}C exposure ages reported from Mt Murphy that do not reproduce at 1σ and 2σ to an unexplained issue with some of the initial in situ ^{14}C measurements, which appears to have been rectified for the replicates. Our results highlight the need to perform replicate analyses when measuring in situ ^{14}C concentrations, and to fully investigate and quantify scatter in in situ ^{14}C datasets.

Several factors may contribute to the low in situ ^{14}C reproducibility observed in this study and require further investigation. These include long term blank variability within in situ ^{14}C extraction facilities and differences in CRONUS-A measurements between in situ ^{14}C extraction laboratories. Quantifying the excess scatter in in situ ^{14}C measurements observed in this study is important because, if used in isolation, in situ ^{14}C exposure ages appear to currently lack the precision needed to reconstruct Holocene deglacial histories at sub-millennial resolution.

Code and data availability. Some of the in situ ^{14}C data examined in this study were obtained from the informal cosmogenic-nuclide exposure age database (ICE-D) and remain unpublished. These data are, however, freely available in ICE-D under the public release requirements of the National Science Foundation (NSF) U.S. Antarctic Program which requires data be made publicly available 2 years after collection. In situ ^{14}C AMS and exposure age data shown in Table 1 are publicly accessible in the UK Polar Data Centre https://doi.org/10.5285/dbb30962-bbf3-434a-9f27-6de2f61a86e2 (Adams et al., 2024).

Supplement. The supplement related to this article is available online at https://doi.org/10.5194/gchron-8-255-2026-supplement.

Author contributions. The author contributions, following the CRediT authorship guidelines, are as follows – conceptualization: JRA, DHR, JSJ; methodology: JRA, DHR; validation: JRA, DHR; analysis: JRA, DHR; investigation: JRA, DHR, JSJ; resources: DHR, SJR, JSJ: data curation: JRA, DHR; original draft: JRA, DHR; review and editing: JRA, DHR, KW, SJR, JSJ: visualization: JRA; supervision: DHR, SJR, JSJ; administration: JRA, DHR, JSJ; funding acquisition: DHR, JSJ.

Competing interests. The contact author has declared that none of the authors has any competing interests.

Disclaimer. Publisher's note: Copernicus Publications remains neutral with regard to jurisdictional claims made in the text, published maps, institutional affiliations, or any other geographical representation in this paper. The authors bear the ultimate responsibility for providing appropriate place names. Views expressed in the text are those of the authors and do not necessarily reflect the views of the publisher.

Acknowledgements. This work is from the "Geological History Constraints" GHC project, a component of the International Thwaites Glacier Collaboration (ITGC). Support was from National Science Foundation (NSF: grant OPP-1738989) and Natural Environment Research Council (NERC: grant NE/S006710/1, NE/S006753/1, NE/K011278/1 and NE/K012088/1). Logistics were provided by NSF-U.S. Antarctic Program and NERC-British Antarctic Survey. We acknowledge Mark Evans for assistance with rock sample preparation, Ryan Venturelli and Brent Goehring for performing the in situ ^{14}C extractions at Tulane Cosmogenic Nuclide Laboratory and Greg Balco for assistance with subsurface in situ ^{14}C–^{10}Be production rate modelling and helpful advice on the manuscript. We also thank Keir Nichols for helpful advice on the manuscript. We would also like to thank the anonymous reviewers for their thorough assessments and helpful suggestions that have strengthened the manuscript. JRA would also like to credit his PhD examiners Derek Fabel and Yves Plancherel for thoughtful and encouraging discussions regarding this research. This is ITGC contribution No. ITGC-163.

Financial support. This research has been supported by the Natural Environment Research Council (grant nos. NE/S006710/1, NE/S006753/1, NE/K012088/1, and NE/K011278/1) and the Directorate for Geosciences (grant no. OPP-1738989).

Review statement. This paper was edited by Philippa Ascough and reviewed by four anonymous referees.

References

Adams, J. R., Johnson, J. S., Roberts, S. J., Mason, P. J., Nichols, K. A., Venturelli, R. A., Wilcken, K., Balco, G., Goehring, B., Hall, B., Woodward, J., and Rood, D. H.: New ^{10}Be exposure ages improve Holocene ice sheet thinning history near the grounding line of Pope Glacier, Antarctica, The Cryosphere, 16, 4887–4905, https://doi.org/10.5194/tc-16-4887-2022, 2022.

Adams, J. R., Venturelli, R. A., Goehring, B. M., Johnson, J. S., Roberts, S. J., and Rood, D. H.: Cosmogenic in situ ^{14}C data and calculated surface exposure ages for 9 erratic cobbles collected from Mount Murphy, West Antarctica, UK Polar Data Centre [data set], https://doi.org/10.5285/dbb30962-bbf3-434a-9f27-6de2f61a86e2, 2024.

Adams, J. R., Mason, P. J., Roberts, S. J., Rood, D. H., Smellie, J. L., Nichols, K. A., Woodward, J., and Johnson, J. S.: Remote Mapping of Bedrock for Future Cosmogenic Nuclide Exposure Dating Studies in Unvisited Areas of Antarctica, Remote Sens.-Basel, 17, https://doi.org/10.3390/rs17020314, 2025.

Argento, D. C., Stone, J. O., Reedy, R. C., and O'Brien, K.: Physics-based modeling of cosmogenic nuclides part I – Radiation transport methods and new insights, Quat. Geochronol., 26, 29–43, https://doi.org/10.1016/j.quageo.2014.09.004, 2015a.

Argento, D. C., Stone, J. O., Reedy, R. C., and O'Brien, K.: Physics-based modeling of cosmogenic nuclides part II – Key aspects of in-situ cosmogenic nuclide production, Quat. Geochronol., 26, 44–55, https://doi.org/10.1016/j.quageo.2014.09.005, 2015b.

Balco, G.: Contributions and unrealized potential contributions of cosmogenic-nuclide exposure dating to glacier chronology, 1990–2010, Quaternary Sci. Rev., 30, 3–27, https://doi.org/10.1016/j.quascirev.2010.11.003, 2011.

Balco, G.: Production rate calculations for cosmic-ray-muon-produced ^{10}Be and ^{26}Al benchmarked against geological calibration data, Quat. Geochronol., 39, 150–173, https://doi.org/10.1016/j.quageo.2017.02.001, 2017.

Balco, G.: Glacier Change and Paleoclimate Applications of Cosmogenic-Nuclide Exposure Dating, Annu. Rev. Earth Pl. Sc., 48, https://doi.org/10.1146/annurev-earth-081619-052609, 2020a.

Balco, G.: Technical note: A prototype transparent-middle-layer data management and analysis infrastructure for cosmogenic-nuclide exposure dating, Geochronology, 2, 169–175, https://doi.org/10.5194/gchron-2-169-2020, 2020b.

Balco, G. and Schaefer, J. M.: Exposure-age record of Holocene ice sheet and ice shelf change in the northeast Antarctic Peninsula, Quaternary Sci. Rev., 59, 101–111, https://doi.org/10.1016/j.quascirev.2012.10.022, 2013.

Balco, G., Stone, J. O., Lifton, N. A., and Dunai, T. J.: A complete and easily accessible means of calculating surface exposure ages or erosion rates from ^{10}Be and ^{26}Al measurements, Quat. Geochronol., 3, 174–195, https://doi.org/10.1016/j.quageo.2007.12.001, 2008.

Balco, G., Todd, C., Goehring, B. M., Moening-Swanson, I., and Nichols, K.: Glacial geology and cosmogenic-nuclide exposure ages from the Tucker Glacier – Whitehall Glacier confluence, Northern Victoria Land, Antarctica, Am. J. Sci., 319, 255–286, https://doi.org/10.2475/04.2019.01, 2019.

Balco, G., Brown, N., Nichols, K., Venturelli, R. A., Adams, J., Braddock, S., Campbell, S., Goehring, B., Johnson, J. S., Rood, D. H., Wilcken, K., Hall, B., and Woodward, J.: Reversible ice sheet thinning in the Amundsen Sea Embayment during the Late Holocene, The Cryosphere, 17, 1787–1801, https://doi.org/10.5194/tc-17-1787-2023, 2023.

Binnie, S. A., Dewald, A., Heinze, S., Voronina, E., Hein, A., Wittmann, H., von Blanckenburg, F., Hetzel, R., Christl, M., Schaller, M., Léanni, L., ASTER Team, Hippe, K., Vockenhuber, C., Ivy-Ochs, S., Maden, C., Fülöp, R. H., Fink, D., Wilcken, K. M., Fujioka, T., Fabel, D., Freeman, S. P. H. T., Xu, S., Fifield, L. K., Akçar, N., Spiegel, C., and Dunai, T. J.: Preliminary results of CoQtz-N: A quartz reference material for terrestrial in-situ cosmogenic ^{10}Be and ^{26}Al measurements, Nucl. Instrum. Meth. B, 456, 203–212, https://doi.org/10.1016/j.nimb.2019.04.073, 2019.

Borchers, B., Marrero, S., Balco, G., Caffee, M., Goehring, B., Lifton, N., Nishiizumi, K., Phillips, F., Schaefer, J., and Stone, J.: Geological calibration of spallation production rates in the CRONUS-Earth project, Quat. Geochronol., 31, 188–198, https://doi.org/10.1016/j.quageo.2015.01.009, 2016.

Briner, J. P., Lifton, N. A., Miller, G. H., Refsnider, K., Anderson, R., and Finkel, R.: Using in situ cosmogenic ^{10}Be, ^{14}C, and ^{26}Al to decipher the history of polythermal ice sheets on Baffin Island, Arctic Canada, Quat. Geochronol., 19, 4–13, https://doi.org/10.1016/j.quageo.2012.11.005, 2014.

Corbett, L. B., Bierman, P. R., and Rood, D. H.: An approach for optimizing in situ cosmogenic ^{10}Be sample preparation, Quat. Geochronol., 33, 24–34, https://doi.org/10.1016/j.quageo.2016.02.001, 2016.

Corbett, L. B., Bierman, P. R., Brown, T. A., Caffee, M. W., Fink, D., Freeman, S. P. H. T., Hidy, A. J., Rood, D. H., Wilcken, K. M., and Woodruff, T. E.: Clean quartz matters for cosmogenic nuclide analyses: An exploration of the importance of sample purity using the CRONUS-N reference material, Quat. Geochronol., 73, 101403, https://doi.org/10.1016/j.quageo.2022.101403, 2022.

Dunai, T. J.: Cosmogenic Nuclides: Principles, Concepts and Applications in the Earth Surface Sciences, Cambridge University Press, https://doi.org/10.1017/CBO9780511804519, 2010.

Fülöp, R., Wacker, L., and Dunai, T. J.: Progress report on a novel in situ ^{14}C extraction scheme at the University of Cologne, Nucl. Instrum. Meth. B, 361, 20–24, https://doi.org/10.1016/j.nimb.2015.02.023, 2015.

Fülöp, R. H., Naysmith, P., Cook, G. T., Fabel, D., Xu, S., and Bishop, P.: Update on the performance of the SUERC in situ ^{14}C extraction line, Radiocarbon, 52, 1288–1294, 2010.

Fülöp, R.-H., Fink, D., Yang, B., Codilean, A. T., Smith, A., Wacker, L., Levchenko, V., and Dunai, T. J.: The ANSTO – University of Wollongong in-situ ^{14}C extraction laboratory, Nucl. Instrum. Meth. B, 438, 207–213, https://doi.org/10.1016/j.nimb.2018.04.018, 2019.

Goehring, B. M., Schaefer, J. M., Schluechter, C., Lifton, N. A., Finkel, R. C., Jull, A. J. T., Akçar, N., and Alley, R. B.: The Rhone Glacier was smaller than today for most of the Holocene, Geology, 39, 679–682, https://doi.org/10.1130/G32145.1, 2011.

Goehring, B. M., Schimmelpfennig, I., and Schaefer, J. M.: Capabilities of the lamont-doherty earth observatory in situ ^{14}C extraction laboratory updated, Quat. Geochronol., 19, 194–197, https://doi.org/10.1016/j.quageo.2013.01.004, 2014.

Goehring, B. M., Wilson, J., and Nichols, K.: A fully automated system for the extraction of in situ cosmogenic carbon-14 in the Tulane University cosmogenic nuclide laboratory, Nucl. Instrum. Meth. B, 455, 284–292, https://doi.org/10.1016/j.nimb.2019.02.006, 2019a.

Goehring, B. M., Balco, G., Todd, C., Moening-Swanson, I., and Nichols, K.: Late-glacial grounding line retreat in the northern Ross Sea, Antarctica, Geology, 47, 291–294, https://doi.org/10.1130/G45413.1, 2019b.

Goehring, B. M., Menounos, B., Osborn, G., Hawkins, A., and Ward, B.: Reconciling the apparent absence of a Last Glacial Maximum alpine glacial advance, Yukon Territory, Canada, through cosmogenic beryllium-10 and carbon-14 measurements, Geochronology, 4, 311–322, https://doi.org/10.5194/gchron-4-311-2022, 2022.

Gosse, J. C. and Phillips, F. M.: Terrestrial in situ cosmogenic nuclides: Theory and application, Quaternary Sci. Rev., 20, 1475–1560, https://doi.org/10.1016/S0277-3791(00)00171-2, 2001.

Granger, D. E.: A review of burial dating methods using ^{26}Al and ^{10}Be, Special Paper of the Geological Society of America, 415, 1–16, https://doi.org/10.1130/2006.2415(01), 2006.

Hein, A. S., Fogwill, C. J., Sugden, D. E., and Xu, S.: Geological scatter of cosmogenic-nuclide exposure ages in the Shackleton Range, Antarctica: Implications for glacial history, Quat. Geochronol., 19, 52–66, https://doi.org/10.1016/j.quageo.2013.03.008, 2014.

Heyman, J., Applegate, P. J., Blomdin, R., Gribenski, N., Harbor, J. M., and Stroeven, A. P.: Boulder height – exposure age relationships from a global glacial ^{10}Be compilation, Quat. Geochronol., 34, 1–11, https://doi.org/10.1016/j.quageo.2016.03.002, 2016.

Hillebrand, T. R., Stone, J. O., Koutnik, M., King, C., Conway, H., Hall, B., Nichols, K., Goehring, B., and Gillespie, M. K.: Holocene thinning of Darwin and Hatherton glaciers, Antarctica, and implications for grounding-line retreat in the Ross Sea, The Cryosphere, 15, 3329–3354, https://doi.org/10.5194/tc-15-3329-2021, 2021.

Hippe, K.: Constraining processes of landscape change with combined in situ cosmogenic ^{14}C–^{10}Be analysis, Quaternary Sci. Rev., 173, 1–19, https://doi.org/10.1016/j.quascirev.2017.07.020, 2017.

Hippe, K. and Lifton, N. A.: Calculating Isotope Ratios and Nuclide Concentrations for In Situ Cosmogenic ^{14}C Analyses, Radiocarbon, 56, 1167–1174, https://doi.org/10.2458/56.17917, 2014.

Hippe, K., Kober, F., Baur, H., Ruff, M., Wacker, L., and Wieler, R.: The current performance of the in situ ^{14}C extraction line at ETH, Quat. Geochronol., 4, 493–500, https://doi.org/10.1016/j.quageo.2009.06.001, 2009.

Hippe, K., Kober, F., Wacker, L., Fahrni, S. M., Ivy-Ochs, S., Akçar, N., Schlüchter, C., and Wieler, R.: An update on in situ cosmogenic ^{14}C analysis at ETH Zürich, Nucl. Instrum. Meth. B, 294, 81–86, https://doi.org/10.1016/j.nimb.2012.06.020, 2013.

Hippe, K., Ivy-Ochs, S., Kober, F., Zasadni, J., Wieler, R., Wacker, L., Kubik, P. W., and Schlüchter, C.: Chronology of Lateglacial ice flow reorganization and deglaciation in the Gotthard Pass area, Central Swiss Alps, based on cosmogenic ^{10}Be and in situ ^{14}C, Quat. Geochronol., 19, 14–26, https://doi.org/10.1016/j.quageo.2013.03.003, 2014.

Jeong, A., Il, J., Bae, Y., Balco, G., Yoo, K., Il, H., Domack, E., Hee, H., and Yong, B.: Late Quaternary deglacial history across the Larsen B embayment, Antarctica, Quaternary Sci. Rev., 189, 134–148, https://doi.org/10.1016/j.quascirev.2018.04.011, 2018.

Johnson, J. S., Bentley, M. J., and Gohl, K.: First exposure ages from the Amundsen Sea Embayment, West Antarctica: The Late Quaternary context for recent thinning of Pine Island, Smith, and Pope Glaciers, Geology, 36, 223–226, https://doi.org/10.1130/G24207A.1, 2008.

Johnson, J. S., Bentley, M. J., Smith, J. A., Finkel, R. C., Rood, D. H., Gohl, K., Balco, G., Larter, R. D., and Schaefer, J. M.: Rapid thinning of Pine Island glacier in the early Holocene, Science, 343, 999–1001, https://doi.org/10.1126/science.1247385, 2014.

Johnson, J. S., Roberts, S. J., Rood, D. H., Pollard, D., Schaefer, J. M., Whitehouse, P. L., Ireland, L. C., Lamp, J. L., Goehring, B. M., Rand, C., and Smith, J. A.: Deglaciation of Pope Glacier implies widespread early Holocene ice sheet thinning in the Amundsen Sea sector of Antarctica, Earth Planet. Sc. Lett., 548, 116–501, https://doi.org/10.1016/j.epsl.2020.116501, 2020.

Johnson, J. S., Venturelli, R. A., Balco, G., Allen, C. S., Braddock, S., Campbell, S., Goehring, B. M., Hall, B. L., Neff, P. D., Nichols, K. A., Rood, D. H., Thomas, E. R., and Woodward, J.: Review article: Existing and potential evidence for Holocene grounding line retreat and readvance in Antarctica, The Cryosphere, 16, 1543–1562, https://doi.org/10.5194/tc-16-1543-2022, 2022.

Jones, A. G., Marcott, S. A., Gorin, A. L., Kennedy, T. M., Shakun, J. D., Goehring, B. M., Menounos, B., Clark, D. H., Romero, M., and Caffee, M. W.: Four North American glaciers advanced past their modern positions thousands of years apart in the Holocene, The Cryosphere, 17, 5459–5475, https://doi.org/10.5194/tc-17-5459-2023, 2023.

Jones, R. S., Johnson, J. S., Lin, Y., Mackintosh, A. N., Sefton, J. P., Smith, J. A., Thomas, E. R., and Whitehouse, P. L.: Stability of the Antarctic Ice Sheet during the pre-industrial Holocene, Nature Reviews Earth and Environment, 3, 500–515, https://doi.org/10.1038/s43017-022-00309-5, 2022.

Jull, A. J. T., Scott, E. M., and Bierman, P.: The CRONUS-Earth inter-comparison for cosmogenic isotope analysis, Quat. Geochronol., 26, 3–10, https://doi.org/10.1016/j.quageo.2013.09.003, 2015.

Kingslake, J., Scherer, R. P., Albrecht, T., Coenen, J., Powell, R. D., Reese, R., Stansell, N. D., Tulaczyk, S., Wearing, M. G., and Whitehouse, P. L.: Extensive retreat and re-advance of the West Antarctic Ice Sheet during the Holocene, Nature, 558, 430–434, https://doi.org/10.1038/s41586-018-0208-x, 2018.

Kohl, C. P. and Nishiizumi, K.: Chemical isolation of quartz for measurement of in-situ-produced cosmogenic nuclides, Geochim. Cosmochim. Ac., 56, 3583–3587, https://doi.org/10.1016/0016-7037(92)90401-4, 1992.

Lamp, J. L., Young, N. E., Koffman, T., Schimmelpfennig, I., Tuna, T., Bard, E., and Schaefer, J. M.: Update on the cosmogenic in situ ^{14}C laboratory at the Lamont-Doherty Earth Observatory, Nucl. Instrum. Meth. B, 456, 157–162, https://doi.org/10.1016/j.nimb.2019.05.064, 2019.

Lifton, N. A.: A new extraction technique and production rate estimate for in situ carbon-14 in quartz, Ph.D thesis, The University of Arizona, http://hdl.handle.net/10150/289000 (last access: 11 September 2025), 1997.

Lifton, N. A., Jull, A. J. T., and Quade, J.: A new extraction technique and production rate estimate for in situ cosmogenic ^{14}C in quartz, Geochim. Cosmochim. Ac., 65, 1953–1969, https://doi.org/10.1016/S0016-7037(01)00566-X, 2001.

Lifton, N., Sato, T., and Dunai, T. J.: Scaling in situ cosmogenic nuclide production rates using analytical approximations to atmospheric cosmic-ray fluxes, Earth Planet. Sc. Lett., 386, 149–160, https://doi.org/10.1016/j.epsl.2013.10.052, 2014.

Lifton, N., Caffee, M., Finkel, R., Marrero, S., Nishiizumi, K., Phillips, F. M., Goehring, B., Gosse, J., Stone, J., Schaefer, J., Theriault, B., Jull, A. J. T., and Fifield, K.: In situ cosmogenic nuclide production rate calibration for the CRONUS-Earth project from lake Bonneville,

Utah, shoreline features, Quat. Geochronol., 26, 56–69, https://doi.org/10.1016/j.quageo.2014.11.002, 2015a.

Lifton, N., Goehring, B., Wilson, J., Kubley, T., and Caffee, M.: Nucl. Instrum. Meth. B, Progress in automated extraction and purification of in situ from quartz: Results from the Purdue in situ ^{14}C laboratory, Nucl. Instrum Meth. B, 361, 381–386, https://doi.org/10.1016/j.nimb.2015.03.028, 2015b.

Lifton, N., Wilson, J., and Koester, A.: Technical note: Studying lithium metaborate fluxes and extraction protocols with a new, fully automated in situ cosmogenic ^{14}C processing system at PRIME Lab, Geochronology, 5, 361–375, 2023.

Longworth, B. E., Von Reden, K. F., Long, P., and Roberts, M. L.: A high output, large acceptance injector for the NOSAMS Tandetron AMS system, Nucl. Instrum. Meth. B, 361, 211–216, https://doi.org/10.1016/j.nimb.2015.04.005, 2015.

Lupker, M., Hippe, K., Wacker, L., Kober, F., Maden, C., Braucher, R., Bourlès, D., Romani, J. R. V., and Wieler, R.: Depth-dependence of the production rate of in situ ^{14}C in quartz from the Leymon High core, Spain, Quat. Geochronol., 28, 80–87, https://doi.org/10.1016/j.quageo.2015.04.004, 2015.

Lupker, M., Hippe, K., Wacker, L., Steinemann, O., Tikhomirov, D., Maden, C., Haghipour, N., and Synal, H. A.: In-situ cosmogenic ^{14}C analysis at ETH Zürich: Characterization and performance of a new extraction system, Nucl. Instrum. Meth. B, 457, 30–36, https://doi.org/10.1016/J.NIMB.2019.07.028, 2019.

Mackintosh, A., White, D., Fink, D., Gore, D. B., Pickard, J., and Fanning, P. C.: Exposure ages from mountain dipsticks in Mac. Robertson Land, East Antarctica, indicate little change in ice-sheet thickness since the Last Glacial Maximum, Geology, 35, 551–554, https://doi.org/10.1130/G23503A.1, 2007.

Marrero, S. M., Phillips, F. M., Borchers, B., Lifton, N., Aumer, R., and Balco, G.: Cosmogenic nuclide systematics and the CRONUScalc program, Quat. Geochronol., 31, 160–187, https://doi.org/10.1016/j.quageo.2015.09.005, 2016.

Merchel, S., Bremser, W., Akhmadaliev, S., Arnold, M., Aumaître, G., Bourlès, D. L., Braucher, R., Caffee, M., Christl, M., Fifield, L. K., Finkel, R. C., Freeman, S. P. H. T., Ruiz-Gómez, A., Kubik, P. W., Martschini, M., Rood, D. H., Tims, S. G., Wallner, A., Wilcken, K. M., and Xu, S.: Quality assurance in accelerator mass spectrometry: Results from an international round-robin exercise for ^{10}Be, Nucl. Instrum. Meth. B, 289, 68–73, https://doi.org/10.1016/j.nimb.2012.07.038, 2012.

Milillo, P., Rignot, E., Rizzoli, P., Scheuchl, B., Mouginot, J., Bueso-Bello, J. L., Prats-Iraola, P., and Dini, L.: Rapid glacier retreat rates observed in West Antarctica, Nat. Geosci., 15, 48–53, https://doi.org/10.1038/S41561-021-00877-Z, 2022.

Nichols, K. A. and Goehring, B. M.: Isolation of quartz for cosmogenic in situ ^{14}C analysis, Geochronology, 1, 43–52, https://doi.org/10.5194/gchron-1-43-2019, 2019.

Nichols, K. A., Goehring, B. M., Balco, G., Johnson, J. S., Hein, A. S., and Todd, C.: New Last Glacial Maximum ice thickness constraints for the Weddell Sea Embayment, Antarctica, The Cryosphere, 13, 2935–2951, https://doi.org/10.5194/tc-13-2935-2019, 2019.

Nichols, K. A., Adams, J. R., Brown, K., Creel, R. C., McKenzie, M. A., Venturelli, R. A., Johnson, J. S., Rood, D. H., Wilcken, K., Woodward, J., and Roberts, S. J.: Direct Geologic Constraints on the Timing of Late Holocene Ice Thickening in the Amundsen Sea Embayment, Antarctica, Geophys. Res. Lett., 51, https://doi.org/10.1029/2024GL110350, 2024.

Phillips, F. M., Argento, D. C., Balco, G., Caffee, M. W., Clem, J., Dunai, T. J., Finkel, R., Goehring, B., Gosse, J. C., Hudson, A. M., Jull, A. J. T., Kelly, M. A., Kurz, M., Lal, D., Lifton, N., Marrero, S. M., Nishiizumi, K., Reedy, R. C., Schaefer, J., Stone, J. O. H., Swanson, T., and Zreda, M. G.: The CRONUS-Earth Project: A synthesis, Quat. Geochronol., 31, 119–154, https://doi.org/10.1016/j.quageo.2015.09.006, 2016a.

Phillips, F. M., Argento, D. C., Bourlès, D. L., Caffee, M. W., Dunai, T. J., Goehring, B., Gosse, J. C., Hudson, A. M., Jull. A. J. T., Kelly, M. A., Lifton, N., Marrero, S. M., Nishiizumi, K., Reedy, R. C., and Stone, J. O. H.: Where now? Reflections on future directions for cosmogenic nuclide research from the CRONUS Projects, Quaternary Geochronol., 31, 155–159, https://doi.org/10.1016/j.quageo.2015.04.010, 2016b.

Pigati, J. S., Lifton, N. A., Timothy Jull, A. J., and Quade, J.: A simplified In Situ cosmogenic ^{14}C extraction system, Radiocarbon, 52, 1236–1243, https://doi.org/10.1017/S0033822200046324, 2010.

Putnam, A. E., Schaefer, J. M., Barrell, D. J. A., Vandergoes, M., Denton, G. H., Kaplan, M. R., Finkel, R. C., Schwartz, R., Goehring, B. M., and Kelley, S. E.: In situ cosmogenic ^{10}Be production-rate calibration from the Southern Alps, New Zealand, Quat. Geochronol., 5, 392–409, https://doi.org/10.1016/j.quageo.2009.12.001, 2010.

Rand, C. and Goehring B. M.: The distribution and magnitude of subglacial erosion on millennial timescales at Engabreen, Norway. Ann. Glaciol., 60, 73–81, https://doi.org/10.1017/aog.2019.42, 2019.

Rand, C., Jones, R. S., Mackintosh, A. N., Goehring, B., and Lilly, K.: A thicker-than-present East Antarctic Ice Sheet plateau during the Last Glacial Maximum, The Cryosphere, 19, 3681–3691, https://doi.org/10.5194/tc-19-3681-2025, 2025.

Rood, D. H., Hall, S., Guilderson, T. P., Finkel, R. C., and Brown, T. A.: Challenges and opportunities in high-precision Be-10 measurements at CAMS, Nucl. Instrum. Meth. B, 268, 730–732, https://doi.org/10.1016/j.nimb.2009.10.016, 2010.

Rood, D. H., Brown, T. A., Finkel, R. C., and Guilderson, T. P.: Poisson and non-Poisson uncertainty estimations of $^{10}Be/^{9}Be$ measurements at LLNL-CAMS, Nucl. Instrum. Meth. B, 294, 426–429, https://doi.org/10.1016/j.nimb.2012.08.039, 2013.

Santos, G. M., Southon, J. R., Druffel-Rodriguez, K. C., Griffin, S., and Mazon, M.: Magnesium Perchlorate as an Alternative Water Trap in AMS Graphite Sample Preparation: A Report On Sample Preparation at Kccams at the University of California, Irvine, Radiocarbon, 46, 165–173, https://doi.org/10.1017/S0033822200039485, 2004.

Santos, G. M., Mazon, M., Southon, J. R., Rifai, S., and Moore, R.: Evaluation of iron and cobalt powders as catalysts for ^{14}C-AMS target preparation, Nucl. Instrum. Meth. B, 259, 308–315, https://doi.org/10.1016/j.nimb.2007.01.220, 2007.

Sbarra, C. M., Briner, J. P., Graham, B. L., Poinar, K., Thomas, E. K., and Young, N. E.: Evidence for a more extensive Greenland Ice Sheet in southwestern Greenland during the Last Glacial Maximum, Geosphere, 18, 1316–1329, https://doi.org/10.1130/GES02432.1, 2022.

Schimmelpfennig, I., Schaefer, J. M., Goehring, B. M., Lifton, N., Putnam, A. E., and Barrell, D. J. A.: Calibration of the in situ cos-

mogenic ^{14}C production rate in New Zealand's Southern Alps, J. Quaternary Sci., 27, 671–674, https://doi.org/10.1002/jqs.2566, 2012.

Smellie, J. L.: Lithofacies Architecture and Construction of Volcanoes Erupted in Englacial Lakes: Icefall Nunatak, Mount Murphy, Eastern Marie Byrd Land, Antarctica, in: Volcaniclastic Sedimentation in Lacustrine Settings, John Wiley & Sons, Ltd., 7–34, https://doi.org/10.1002/9781444304251.ch2, 2001.

Søndergaard, A. S., Larsen, N. K., Steinemann, O., Olsen, J., Funder, S., Egholm, D. L., and Kjær, K. H.: Glacial history of Inglefield Land, north Greenland from combined in situ ^{10}Be and ^{14}C exposure dating, Clim. Past, 16, 1999–2015, https://doi.org/10.5194/cp-16-1999-2020, 2020.

Southon, J.: Graphite reactor memory – Where is it from and how to minimize it?, Nucl. Instrum. Meth. B, 259, 288–292, https://doi.org/10.1016/j.nimb.2007.01.251, 2007.

Spector, P., Stone, J., Cowdery, S. G., Hall, B., Conway, H., and Bromley, G.: Rapid early-Holocene deglaciation in the Ross Sea, Antarctica, Geophys. Res. Lett., 44, 7817–7825, https://doi.org/10.1002/2017GL074216, 2017.

Spector, P., Stone, J., and Goehring, B.: Thickness of the divide and flank of the West Antarctic Ice Sheet through the last deglaciation, The Cryosphere, 13, 3061–3075, https://doi.org/10.5194/tc-13-3061-2019, 2019.

Stone, J. O., Balco, G. A., Sugden, D. E., Caffee, M. W., Sass, L. C., Cowdery, S. G., and Siddoway, C.: Holocene deglaciation of Marie Byrd Land, West Antarctica, Science, 299, 99–102, https://doi.org/10.1126/science.1077998, 2003.

Stutz, J., Mackintosh, A., Norton, K., Whitmore, R., Baroni, C., Jamieson, S. S. R., Jones, R. S., Balco, G., Salvatore, M. C., Casale, S., Lee, J. I., Seong, Y. B., McKay, R., Vargo, L. J., Lowry, D., Spector, P., Christl, M., Ivy Ochs, S., Di Nicola, L., Iarossi, M., Stuart, F., and Woodruff, T.: Mid-Holocene thinning of David Glacier, Antarctica: chronology and controls, The Cryosphere, 15, 5447–5471, https://doi.org/10.5194/tc-15-5447-2021, 2021.

Venturelli, R. A., Siegfried, M. R., Roush, K. A., Li, W., Burnett, J., Zook, R., Fricker, H. A., Priscu, J. C., Leventer, A., and Rosenheim, B. E.: Mid-Holocene Grounding Line Retreat and Readvance at Whillans Ice Stream, West Antarctica, Geophys. Res. Lett., 47, https://doi.org/10.1029/2020GL088476, 2020.

Venturelli, R. A., Boehman, B., Davis, C., Hawkings, J. R., Johnston, S. E., Gustafson, C. D., Michaud, A. B., Mosbeux, C., Siegfried, M. R., Vick-Majors, T. J., Galy, V., Spencer, R. G. M., Warny, S., Christner, B. C., Fricker, H. A., Harwood, D. M., Leventer, A., Priscu, J. C., and Rosenheim, B. E.: Constraints on the Timing and Extent of Deglacial Grounding Line Retreat in West Antarctica, AGU Advances, 4, 1–15, https://doi.org/10.1029/2022AV000846, 2023.

White, D., Fülöp, R. H., Bishop, P., Mackintosh, A., and Cook, G.: Can in-situ cosmogenic ^{14}C be used to assess the influence of clast recycling on exposure dating of ice retreat in Antarctica?, Quat. Geochronol., 6, 289–294, https://doi.org/10.1016/j.quageo.2011.03.004, 2011.

Wilcken, K. M., Codilean, A. T., Fülöp, R.-H., Kotevski, S., Rood, A. H., Rood, D. H., Seal, A. J., and Simon, K.: Technical note: Accelerator mass spectrometry of ^{10}Be and ^{26}Al at low nuclide concentrations, Geochronology, 4, 339–352, https://doi.org/10.5194/gchron-4-339-2022, 2022.

Young, N. E., Schaefer, J. M., Briner, J. P., and Goehring, B. M.: A ^{10}Be production-rate calibration for the Arctic, J. Quaternary Sci., 28, 515–526, https://doi.org/10.1002/jqs.2642, 2013.

Young, N. E., Schaefer, J. M., Goehring, B., Lifton, N., Schimmelpfennig, I., and Briner, J. P.: West Greenland and global in situ ^{14}C production-rate calibrations, J. Quaternary Sci., 29, 401–406, https://doi.org/10.1002/jqs.2717, 2014.

Young, N. E., Lesnek, A. J., Cuzzone, J. K., Briner, J. P., Badgeley, J. A., Balter-Kennedy, A., Graham, B. L., Cluett, A., Lamp, J. L., Schwartz, R., Tuna, T., Bard, E., Caffee, M. W., Zimmerman, S. R. H., and Schaefer, J. M.: In situ cosmogenic ^{10}Be–^{14}C–^{26}Al measurements from recently deglaciated bedrock as a new tool to decipher changes in Greenland Ice Sheet size, Clim. Past, 17, 419–450, https://doi.org/10.5194/cp-17-419-2021, 2021.